Monthly Notices of the ROYAL ASTRONOMICAL SOCIETY

MNRAS **520,** 5413–5432 (2023) https://doi.org/10.1093/mnras/stad407
Advance Access publication 2023 February 14

A survey for variable young stars with small telescopes: VI – Analysis of the outbursting Be stars NSW 284, gaia 19eyy, and VES 263

Dirk Froebrich ,[1★†‡] Lynne A. Hillenbrand,[2] Carys Herbert ,[3] Kishalay De,[4] Jochen Eislöffel,[5] Justyn Campbell-White,[6,7] Ruhee Kahar,[3,7] Franz-Josef Hambsch,[8,9,10] Thomas Urtly,[11] Adam Popowicz,[12] Krzysztof Bernacki,[12] Andrzej Malcher,[12] Slawomir Lasota,[12] Jerzy Fiolka,[12] Piotr Jozwik-Wabik,[12] Franky Dubois,[8,13] Ludwig Logie,[8,13] Steve Rau,[8,13] Mark Phillips,[10,11,14] George Fleming,[11] Rafael Gonzalez Farfán,[15,16] Francisco C. Soldán Alfaro,[10,15,17] Tim Nelson,[18,19] Stephen R.L. Futcher,[11,18,20] Samantha M. Rolfe,[21] David A. Campbell,[21] Tony Vale,[10,11,22,23,24] Pat Devine,[14] Dawid Moździerski,[25] Przemysław J. Mikołajczyk,[25,26] Heinz-Bernd Eggenstein,[27] Diego Rodriguez,[10] Ivan L Walton,[11] Siegfried Vanaverbeke,[8,13,28] Barry Merrikin,[18] Yenal Öğmen,[29] Alex Escartin Perez,[15] Mario Morales Aimar,[15,30] Georg Piehler,[31] Lord Dover,[3] Aashini L. Patel,[3] Niall Miller,[3,32] Jack Finch,[3] Matt Hankins,[33] Anna M. Moore,[34] Tony Travouillon[34] and Marek Szczepanski[35]

Affiliations are listed at the end of the paper

Accepted 2023 February 3. Received 2023 February 3; in original form 2022 September 13

ABSTRACT

This paper is one in a series reporting results from small telescope observations of variable young stars. Here, we study the repeating outbursts of three likely Be stars based on long-term optical, near-infrared, and mid-infrared photometry for all three objects, along with follow-up spectra for two of the three. The sources are characterized as rare, truly regularly outbursting Be stars. We interpret the photometric data within a framework for modelling light-curve morphology, and find that the models correctly predict the burst shapes, including their larger amplitudes and later peaks towards longer wavelengths. We are thus able to infer the start and end times of mass loading into the circumstellar discs of these stars. The disc sizes are typically 3 – 6 times the areas of the central star. The disc temperatures are ∼40 per cent, and the disc luminosities are ∼10 per cent of those of the central Be star, respectively. The available spectroscopy is consistent with inside-out evolution of the disc. Higher excitation lines have larger velocity widths in their double-horned shaped emission profiles. Our observations and analysis support the decretion disc model for outbursting Be stars.

Key words: techniques: photometric – stars: early-type – stars: emission-line, Be – stars: mass-loss.

1 INTRODUCTION

Classical Be stars have long been recognized as objects in the later main sequence or early post-main sequence stage of evolution that are rapidly rotating (Slettebak 1982). By definition they are early-type stars exhibiting emission lines, typically H α that is double-peaked though a wide range of line profiles is presented, as well as some higher Balmer series lines and occasionally also He I and/or Fe II (Slettebak, Collins & Truax 1992). Be stars generally have weak near-infrared excesses consistent with free–free emission (Finkenzeller & Mundt 1984) and can be detected in the radio. The ‘classical Be’ nomenclature distinguishes them from Be phenomena arising due to binary interactions among evolved massive stars.

Classical Be star spin rates are close enough to the breakup velocity (> 70 per cent; Porter 1996) that their observed properties are interpreted as being due to equatorial mass-loss that produces a decretion disc[1] (as opposed to an accretion disc). The discs are thought to be dust-free, and the gas emission is constrained from observed line widths to arise in the inner few stellar radii. Rivinius, Carciofi & Martayan (2013) provides a general review of the Be phenomenon, and describes ‘an outwardly diffusing gaseous Keplerian disc [...] fed by mass ejected from the central star [...] and governed by viscosity’.

A fraction of the classical Be population undergoes outburst behaviour. Although several mechanisms for putting material into the surrounding disc have been suggested, the currently favoured hypothesis is a non-radial pulsation-driven means (e.g. Ressler 2021,

★ E-mail: df@kent.ac.uk
† HOYS Observer
‡ Observer Beacon Observatory

[1] Older literature, including the original proposal by Lee, Osaki & Saio (1991) uses the term ‘excretion disc’.

and references therein). The combination of rapid stellar rotation, presumably inherited from the main sequence, the radius inflation that occurs during post-main sequence evolution, and the existence of an outburst mechanism, leads to the star exceeding its breakup velocity, and hence to equatorial mass-loss that replenishes the disc from the inside. In the assumed viscous disc scenario, the addition of material at the inner disc edge implies transport of both mass and angular momentum outwards. According to Rivinius et al. (2013), when the mass addition at the inner edge ceases, the sense of the mass flow reverses and the star can re-accrete any remaining disc material that has not otherwise escaped the system.

A well-known Be star data base is described by Neiner et al. (2011). Over the decades, various H α surveys, including IPHAS (Drew et al. 2005), have continued to identify candidate Be stars. Recently, large-scale spectroscopic surveys such as APOGEE (Chojnowski et al. 2015) and LAMOST (e.g. Wang et al. 2022) have contributed as well. The observational properties of Be stars, and indeed the ratio of Be to non-Be is roughly dependent on spectral-type, with typical divisions into early (B0 – B3), mid (B4 – B7), and late (B8 – B9) type Be stars.

The Be stars are also ubiquitous photometric variables. They have been studied as such from the ground e.g. using OGLE (Mennickent et al. 2002), KELT (Labadie-Bartz et al. 2017a), and ASAS (Bernhard et al. 2018). Studies at high precision and cadence have used CoRoT (Semaan et al. 2018), *Kepler* (Rivinius, Baade & Carciofi 2016; Labadie-Bartz et al. 2017), and *TESS* (Labadie-Bartz et al. 2022). Variability types include stellar pulsation (both low-order g modes and higher frequency p modes), other clustered periodic modes, stochastic photometric behaviour that is attributed to discs, discrete outbursts, and finally, long-term trends. Labadie-Bartz et al. (2018) again working with KELT data, conducted a Be variability study focused on the outbursting category.

Mennickent et al. (2002) had earlier identified two families of outburst light curves: sharp and hump-like, and had found 13 per cent of the Be star sample to exhibit outbursts. Labadie-Bartz et al. (2017) found a higher 36 per cent of Be stars to exhibit outbursts, while Labadie-Bartz et al. (2018) from the same data set state 28 per cent. Labadie-Bartz et al. (2022), using space-based *TESS*, find a similar 31 per cent of their Be star sample to show 'bursts', with sensitivity that allows identification of shorter duration and much lower amplitude bursts than would be detected as 'outbursts' in ground-based photometry. Bernhard et al. (2018), however, find a much more sizable 3/4 of their Be star sample to show 'bursts'. Both Labadie-Bartz and Bernhard demonstrate a spectral type dependence, with earlier type Be stars having a higher burst frequency. The burst amplitude and duration are again correlated with the spectral class, in the sense of being larger and longer for the earlier type Be stars. Further, both authors quantify the burst rise times and decay times, with the latter being typically 2–3 times the former. Concerning the burst frequency, as these authors use different definitions of burst behaviour (including negative departures from baseline brightness which are interpreted as outbursts seen through an edge-on disc and therefore dimming rather than brightening events), and may cover different parts of the B spectral type range differently, it is unclear what to make of the factors of several differences in the reported percentages (13 per cent versus about 30 per cent versus 73 per cent).

Our main interest is in the long duration, discrete outburst events. Such outbursting behaviour is recurrent, and reported as somewhere between irregular (Rivinius et al. 2013) and semiregular (Labadie-Bartz et al. 2017; Bernhard et al. 2018), with reported rates of 0.5–5 per year per outbursting Be star. Recent examples of in-depth studies of individual outbursting Be sources are those of Richardson et al. (2021) focusing on spectroscopy (see also the spectral time-series of several objects shown in Labadie-Bartz et al. 2018), and Ghoreyshi et al. (2018) focusing on photometry. Detailed light-curve modelling is also reported by Rímulo et al. (2018).

In this paper, we identify three newly recognized early-spectral class Be stars, as having repeating photometric and spectroscopic outbursts. The bursts are hump-like, occur on time-scales of less than a year, and have visual amplitudes of up to 0.5 mag. We discuss the three stars in Section 2, report the long-term photometric monitoring in Section 3, as well as spectroscopy in Section 4 of two of the three, that confirms the Be status and covers low and high states. In Section 5 we discuss our fit of the photometric outbursts with a simple model to determine the temperature and surface area of the emitting material. Finally, we discuss our findings in Section 6.

2 THE STARS

The three sources under study here are NSW 284, Gaia 19eyy, and VES 263, each of which is described below. Table 1 provides other identifiers, Gaia DR3 astrometry, photometry, and estimated stellar parameters including distance, extinction, spectral type, etc. (Gaia Collaboration 2016, 2022). Each of these three sources has a spectral energy distribution consistent with an early spectral type stellar photosphere, with no or only minor infrared excess.

2.1 NSW 284

This source is in Cepheus, projected into the south of the IC 1396 HII region, but a far background object according to the GaiaDR3 distance of about 5.3 kpc. It was identified as an H α emission-line star by Nakano et al. (2012) and first presented as a variable star by Froebrich et al. (2018) who assumed it was a YSO. Here, we recognize the source as a Be star rather than a YSO. Table 1 provides its parameters. Reddening of $E(B - V) = 1.16 \pm 0.56$ mag (Carvalho & Hillenbrand 2022) combined with the *Gaia G*-band magnitude suggests an early B spectral type, consistent with our spectroscopic determination below that it is a B3 type star. However, the measured *B–V* colour outside of the photometric bursts is about 0.70–0.75 mag, while APASS reports $B - V = (15.043 \pm 0.003) - (14.206 \pm 0.007) = 0.8$ mag; in either case a negative intrinsic colour results, $(B - V)_0 < -0.3$ mag, suggesting an early O-type star. An alternate to this scenario is that strong Balmer continuum emission originating in hot circumstellar gas causes a blue-ing, even in the out-of-burst light curve.

2.2 Gaia 19eyy

Located in Puppis, this source has no previous literature despite being characterized on the Gaia Alerts page[2] as a YSO. Here, we analyse the source as a Be star outburster rather than a YSO based on the light-curve similarity to NSW 284 and VES 263. The GaiaDR3 distance is about 6 kpc and the extinction is unknown. As can be seen in Table 1, the apparent optical colours of Gaia 19eyy during quiescence are almost identical to NSW 284. Together with the similar distance, absolute *Gaia* magnitude and light-curve behaviour, we infer that the source closely resembles a Be type source, despite the absence of spectroscopic confirmation.

[2] http://gsaweb.ast.cam.ac.uk/alerts/alert/Gaia19eyy/

Table 1. Adopted and determined properties of the three sources. We list the GaiaDR3 astrometry and stellar parameters, other literature values for the stellar parameters, average baseline magnitudes, and colours from HOYS, and the typical burst properties. The references for the literature stellar parameters are as follows: (1) Carvalho & Hillenbrand (2022); (2) Munari et al. (2019); (3) This work; (4) Comerón & Pasquali (2012).

Name	NSW 284	Gaia 19eyy	VES 263
Aliases	[NSW2012] 284		SS 447
	PTFS 1821n		Gaia18azl
GaiaDR3 astrometry			
RA (J2000)	21 38 39.81	08 30 42.50	20 31 48.85
Dec (J2000)	+ 57 08 47.1	−41 33 42.6	+ 40 38 00.1
p (mas)	0.1880 [0.0153]	0.1626[0.0122]	0.5733 [0.0105]
d (kpc)	5.32	6.15	1.74
RUWE	1.155	0.956	1.113
μ_α (mas yr^{-1})	−2.549 [0.019]	−2.773 [0.013]	−2.951 [0.011]
μ_δ (mas yr^{-1})	−2.093 [0.018]	3.411[0.013]	−5.336 [0.012]
GaiaDR3 stellar parameters			
T (K)	22 666 [1,000]	15 415 [200]	–
log g (cm s^{-2})	4.24 [0.12]	3.70 [0.03]	–
A_V (mag)	2.9	2.6	–
M_G (mag)	−1.66	−1.62	–
Literature stellar parameters			
A_V (mag)	3.6 [1.7]$^{(1)}$		4.1 [1.9]/5.6 [0.15]$^{(1, 2)}$
SpT	∼B3e$^{(3)}$		B1 II$^{(4)}$
T (K)	17,500$^{(3)}$	17,500$^{(3)}$	20,666$^{(4)}$
L [L$_\odot$]			13 000 [1000]$^{(2)}$
M [M$_\odot$]			9.1/12$^{(2, 4)}$
Average baseline magnitudes from this work			
B (mag)	15.50	14.29	14.92
V (mag)	14.76	13.53	13.10
R (mag)	14.57	13.31	12.07
I (mag)	14.29	13.05	11.06
Average baseline colours from this work			
B–V (mag)	0.74	0.76	1.82
V–R (mag)	0.19	0.22	1.03
R–I (mag)	0.28	0.26	1.01
Typical burst characteristics from this work			
cadence (d)	280–390	390–490	140–190
duration (d)	200	150	120
R amp (mag)	<0.6	<0.6	<0.5

2.3 VES 263

This source is in Cygnus and is a strong emission-line object that has appeared in many H α catalogues over the decades (e.g. Kohoutek & Wehmeyer 1997, but see Munari et al. 2019 for older references). The star was determined by Berlanas et al. (2019) to be a kinematic member of Cyg OB2, at mean distance 1760 pc, a result independently confirmed by Munari et al. (2019). It was previously suggested as such by Comerón & Pasquali (2012) who assigned a spectral type of B1 II and derived $A_V = 4.4$ mag, as well as the other stellar parameters reported in Table 1. Munari et al. (2019) find $E(B - V) = 1.80 \pm 0.05$ mag from spectral energy distribution (SED) fitting. From DIBs analysis, Carvalho & Hillenbrand (2022) found an extinction value of $E(B - V) = 1.33 \pm 0.61$ mag, consistent with the Comerón & Pasquali (2012) value of A_V for an $R_V = 3.1$ as well as the DIBs measurements in Munari et al. (2019) but marginally lower than the SED fitting value in Munari et al. (2019). The only paper discussing VES 263 in any depth is Munari et al. (2019), who present the source based on a *Gaia* Alert[3] as an eruptive Herbig Ae/Be star. These authors assembled the historical record, which includes an approximately 10-yr high state from ∼1955 to 1965 and their follow-up photometry and spectroscopy of the 2018 brightening of the photometric baseline that was reported by *Gaia*. Rather than a pre-main sequence star, here we suggest that VES 263 is instead an evolved Be star undergoing outbursts.

3 PHOTOMETRY AND LONG-TERM LIGHT CURVES

We have assembled a comprehensive set of photometric data for each of the three sources, with Fig. 1 displaying the composite multiwavelength light curves. In this section, we discuss the data sets and describe the long-term light curves.

3.1 HOYS photometry

The vast majority of the optical photometry data of NSW 284 and Gaia 19eyy, used in our analysis, has been obtained as part of the Hunting Outbursting Young Stars (HOYS) citizen science project (Froebrich et al. 2018). This project observes a number of young, nearby clusters and star forming regions in optical filters with amateur telescopes. The HOYS observations for NSW 284 are taken by a wide variety of observatories due to the nature of the project (Froebrich et al. 2018; Evitts et al. 2020). The southern position of the Gaia 19eyy source means that all data are taken by the same observatory, the Remote Observatory Atacama Desert (ROAD; Hambsch 2012).

All HOYS target fields have deep images in all optical filters taken under photometric conditions as reference for relative photometry. The off-sets of the instrumental magnitudes in the reference images to the B, V, R_c, I_c system (the filters used for the reference images) have been obtained with the Cambridge Photometric Calibration Server.[4] For simplicity we refer to the Cousins filters as R and I, throughout the paper. For each HOYS target field we identify non-variable stars in our vast data set. Their colours and magnitudes are used to determine the colour terms in each image and correct them. The full details of this procedure can be found in Evitts et al. (2020). It is those corrected magnitudes we use throughout for the analysis of the light curves.

In Fig. 1 we show the long-term light curves for our sources. They combine the B, V, R, I data from HOYS with optical and infrared photometry from auxiliary data sets discussed in Section 3.2.

3.2 Auxiliary photometry

In addition to the HOYS monitoring photometry, our sources of interest have been included in a number of different time domain surveys. Here, we reference and discuss the additional data that enable us to have a longer term and broader wavelength look at the bursts. All of those are included in the long-term light curves displayed in Fig. 1.

(i) The object VES 263 is not situated in one of the HOYS target fields. Thus, as baseline photometry, we use the B, V, R, and I data from Munari et al. (2019) taken in 2018/19.

[3]http://gsaweb.ast.cam.ac.uk/alerts/alert/Gaia18azl/
[4]`http://gsaweb.ast.cam.ac.uk/followup`

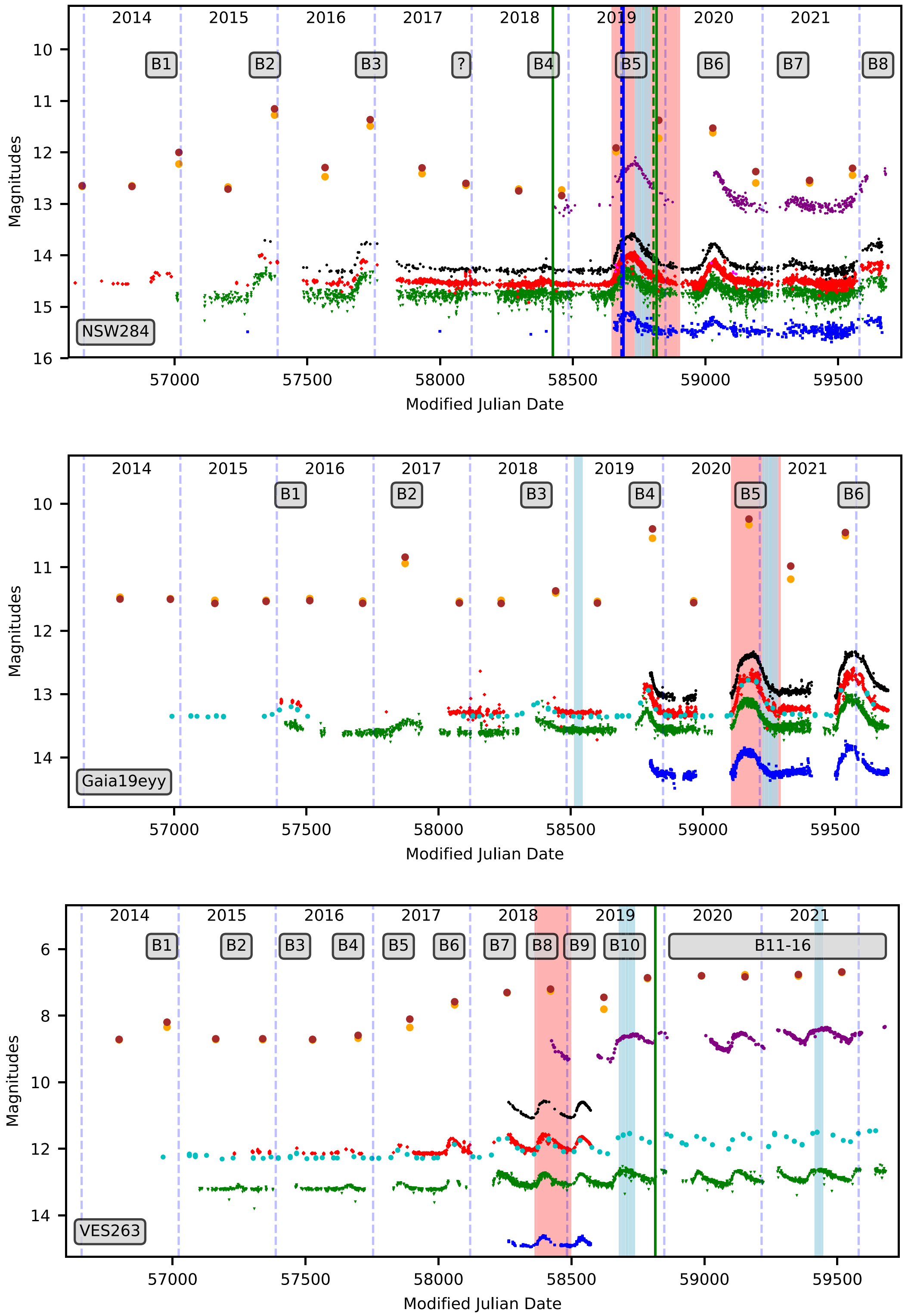

Figure 1. Long-term light curves of NSW 284 (top), Gaia 19eyy (middle), and VES 263 (bottom). Filters from bottom to top are colour coded: *B* – blue, *V* – green, *R* – red, Gmag – turquoise, *I* – black, *J* – purple, *W*1 – orange, *W*2 – brown. The identified bursts are labelled and the '?' indicates a potentially failed burst. The red shaded bursts are discussed as examples in detail in Section 5. The light blue shaded times indicate the *TESS* sectors with data available. The dashed vertical lines indicate January 1st each year. The green vertical lines indicate Keck spectra (solid – HIRES; dashed – NIRSPEC). The blue vertical lines indicate the Palomar 200" spectra (solid – DoubleSpec; dashed – TripleSpec). The optical (*BVRI*) photometry combines data from HOYS, ASAS-SN, ATLAS, PTF, ZTF, and from Munari et al. (2019) for VES 263. If taken in different filters they are manually shifted into the nearest appropriate filter, e.g. g into V (see Section 3.2) for details.

(ii) All three sources have data in the All-Sky Automated Survey for Supernovae (ASAS-SN; Shappee et al. 2014; Kochanek et al. 2017). Photometry is available in the V and g filters. We manually shifted the data in Fig. 1 to match our HOYS V-band photometry. The magnitude off-sets are slightly different for the three sources due to their different colours – notably VES 263 (see Table 1).

(iii) Photometry from the Asteroid Terrestrial-impact Last Alert System (ATLAS; Tonry et al. 2018) is also available for all three sources. Data taken in the c (cyan) and o (orange) filters have been adopted and manually shifted to match the baseline V and R photometry, respectively. The data for VES 263 are very noisy (0.5 mag) after MJD = 58500. These are hence not included in Fig. 1.

(iv) The *Gaia* Alerts (Hodgkin et al. 2021) contain light curves for VES 263 (Gaia18azl) and Gaia 19eyy, but not NSW 284 since it did not trigger an alert. We note that the *Gaia Gmag* filter approximates R for red sources, which is evident in Fig. 1.

(v) The Palomar-Gattini-InfraRed survey (PGIR; Moore & Kasliwal 2019; De et al. 2020) observes the sky every two nights in the near-infrared J-band to a median depth of $J = 15.7$ mag (AB). The J-band light curves are available for NSW 284 and VES 263 beginning on JD = 2458410, but not Gaia 19eyy due to its southerly declination.

(vi) The *WISE* mission (Wright et al. 2010; Cutri & et al. 2012) and the repurposed NEOWISE time domain survey (Mainzer et al. 2011; Cutri et al. 2021) provides all-sky mid-infrared survey data and has light curves in the $W1$ and $W2$ bands for all three of our sources. Although the NEOWISE ∼6-month cadence provides data that are undersampled relative to the variability time-scales, there is detectable brightening in the $W1$ and $W2$ bands that corresponds to the optical bursts. NEOWISE also shows evidence that the burst behaviour occurred before the start of HOYS.

(vii) Palomar Transient Factory (PTF; Law et al. 2009) r-band data are available for NSW 284. We include these data, shifted into our R-band, in the long-term light curve. There are a handful of data points for VES 263, but due to the small number, we have not added them to Fig. 1.

(viii) The Zwicky Transient Factory survey (ZTF; Bellm et al. 2019) has recorded data for NSW 284 in g and r (internal ID = ZTF18abksgkt). For VES 263 only g data are available. They were retrieved from IPAC (Masci et al. 2019) and cover 2018 April through to the present. As for the other surveys, we manually shifted the g and r data into our V and R photometry.

(ix) The *Transiting Exoplanet Survey Satellite* (*TESS*; Ricker et al. 2015) conducted short time-scale monitoring at 30 min cadence of all three sources. At present, each source has two sequential sectors of data available, with a sector spanning 24 – 28 d, and two of the three sources have a third sector that is separated by nearly 2 yr. The photometry has not been added into our long-term light curves in Fig. 1, but the individual sectors are indicated as light blue shaded areas.

3.3 Summary of light-curve behaviour

The light curves shown in Fig. 1 have some common features, but the three sources are also somewhat distinct in their photometric behaviour. All sources show repeated bursts since the start of our data in 2014, with approximately 1 – 2 bursts per year. We have visually identified all bursts (see labels 'B' in Fig. 1). We define as a burst times where the average brightness deviates in a sustained manner by more than the typical photometric scatter from the flat baseline in at least one of the filters. The most salient feature of the light curves is that the burst amplitudes are larger towards redder wavelengths. Furthermore, they tend to peak later at longer wavelengths. Table 1 provides the median burst amplitudes, which are typically several tenths of a mag, and burst durations, which are typically several months. Below we give a brief description of the long-term light curve for each source.

3.3.1 NSW284

The object shows a flat light curve with superimposed bursts (see top panel of Fig. 1). There are in total eight bursts during the 8.5 yr of data. There is a clear gap between B3 and B4 in 2017/18. Based on the behaviour prior and after that, one could have expected a burst to appear at that time. The *WISE* magnitudes in late 2017 are marginally higher (by 0.1 mag, or one sigma) than in the subsequent mid-2018 data point, hinting at a weak burst, which was not detectable in the optical data. We have indicated that gap as '?'. Including the questionable burst, the average gap between bursts is about 345 d, but they range from 280 to 390 d. One can see that prior to the questionable burst the gaps are slightly larger than 1 yr, while afterwards they are shorter and of the order of 330 d.

While B1 is detected only in R and the *WISE* data, the other bursts are consistently covered in the optical data. Starting from 2019 (B5), we have also regular B and J-band photometry. Throughout, the amplitudes in all bursts are higher at longer wavelengths. Similarly, the brightness increase is faster than the decrease and the peak brightness occurs slightly later at longer wavelengths. The burst amplitudes and duration vary from burst to burst. For the stronger bursts the amplitudes range from 0.2 mag in B to almost 2 mag in the *WISE* filters. Lower amplitude bursts appear shorter, probably in part because the declining part of the burst merges into the noise of the data sooner. There is no discernible pattern (within the limited number of bursts detected) that indicates whether a burst is stronger or weaker. The *TESS* data available for this source coincides with one of the declines in brightness (burst B5). Other than a general drop in flux, there are no other discernible features visible in this high cadence data.

3.3.2 Gaia 19eyy

The long-term light curve of Gaia 19eyy, shown in the middle panel of Fig. 1, is similar to NSW 284. There are distinct bursts on top of a low-state brightness. Coverage of the objects at time-scales significantly below the burst duration starts in early 2015. However, we only have good multifilter data since the end of 2019, when the object got flagged up as variable star in the *Gaia* alerts (Hodgkin et al. 2021). Similar to NSW 284 the bursts are semiregular, with six detected bursts over 7.5 yr. Thus, the average cadence is approximately 450 d, with gaps ranging from 390 to 490 d. Again, there is a slight trend that the gaps between bursts decrease over time.

All bursts but B1 and B3 show very strong *WISE* amplitudes. This seems to be caused by timing of the data rather than real differences, as B1 and B3 peak in the optical between two of the *WISE* data points. In contrast to NSW 284, the optical bursts seem to be slightly more symmetric. Hence, the increase and decrease in brightness are of about the same length. The latest three bursts (B4–B6) are clearly stronger than the first three (B1–B3), but we do not think this is a significant trend. Thus, in all aspects the burst and long-term light curves of Gaia 19eyy and NSW 284 are very similar. This includes the *TESS* data available, which does not show any short-term variability.

3.3.3 VES 283

The long-term light curve of VES 263 (shown in the bottom panel of Fig. 1) has aspects similar to the two other objects. However, it also differs significantly. The optical 2018/19 data has been discussed in Munari et al. (2019). We only have long-term coverage in *V* and *Gmag* for the entire duration of the data. The *R* data only covers pre-2018/19 and *J*-band coverage is available from late 2018.

Since 2014, our long-term data indicates a total of 16 bursts. Initially (up to 2018) the bursts appear on top of a flat baseline brightness. Their cadence is approximately 180 d (slightly decreasing) and the amplitudes do appear to increase from burst to burst in *V* and *R*. After 2019 the bursts increase in amplitude and their cadence decreases to about 145 d. Furthermore, the brightness does not return to the pre-2018 baseline magnitudes in-between bursts.

The *WISE* light curve suggests a general, almost 2 mag brightening in the MIR from 2018. Judging by the general increase of the faint state at optical wavelengths discussed above, this might in part be the case. However, it is also evident that the *WISE* observing cadence almost matches the outbursts of this source. Most *WISE* data are taken just after the optical peaks. Given that in the other objects the peak at longer wavelengths occurs later, it is likely that VES 263 still varies in the *WISE* bands, and the steady increase seen in the data is only in part real, and in part caused by the observing cadence.

The *TESS* data for this object show some short-term variations. For about half of the *TESS* coverage, regular variations with a period of about 17 h can by found. The peak-to-peak amplitudes vary from at most 0.7 per cent to zero, i.e. they disappear into the noise. These variations cannot be attributed to surface features or orbiting disc material, as the periods would be much larger. Thus, the most likely source for the variability are pulsations. If these are part of the trigger mechanism for the bursts, or the termination of the mass loading is not clear, as they are not observed in any of the other sources.

4 SPECTROSCOPIC OBSERVATIONS AND FINDINGS

We have obtained a number of spectra for two of our sources, NSW 284 and VES 263, during different parts of the light curve. Below we describe the data and discuss the spectra in detail.

4.1 NSW284

4.1.1 Palomar 200"/DoubleSpec

An optical spectrum was taken on 2019 July 27 with the Palomar 200" telescope and facility optical spectrograph DoubleSpec (Oke & Gunn 1982, in original form). At that time the source was approximately half way through the brightness increase of burst B5. We used the D68 dichroic to separate the spectrograph arms. The source was observed using the 600 l mm^{-1} and 4000 Å blaze (blue), and the 1200 l mm^{-1} and 7100 Å blaze (red) gratings, respectively. Data were processed using standard tasks in IRAF to produce a 1D wavelength and flux-calibrated spectrum between ≈4000 and 9000 Å.

The blue-side spectrum shows strong absorption in the Na I D doublet as well as in the 5780 and 6614 Å (weaker) diffuse interstellar band (DIB) features. There is weak H α emission having an equivalent width $W_\lambda < 2$ Å, but the other Balmer lines are in very weak absorption. The red-side spectrum is essentially featureless, aside from telluric contributions, with no evidence of Paschen line absorption. Although we believe the source to be an early-type star

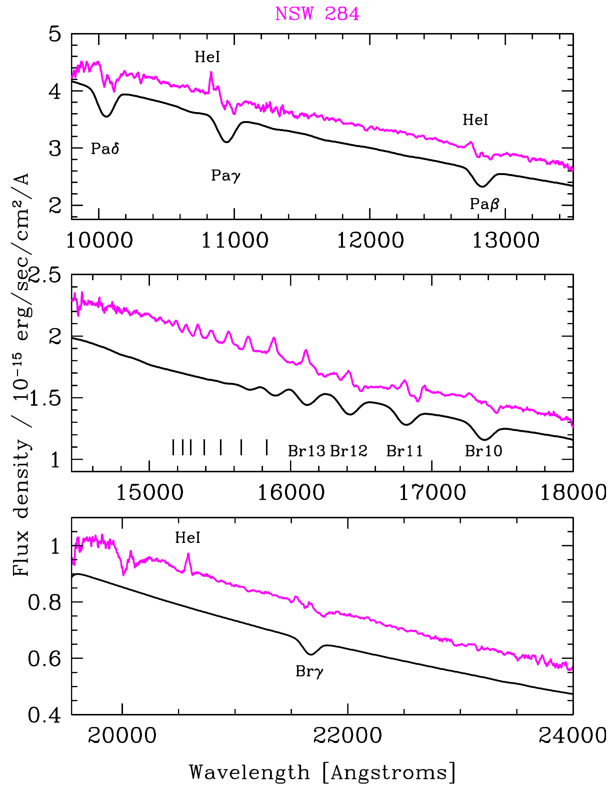

Figure 2. Near-infrared (*JHK*) spectrum of NSW 284 (magenta) taken during the rise of burst B5, compared to a NextGen model spectrum that has been reddened by the extinction value in Table 1, and scaled (black). The spectrum temperature of 9800 K was chosen to highlight the expected locations of the near-infrared hydrogen lines. NSW 284 exhibits a relatively featureless continuum, with only weak H and He emission lines. Paschen signatures at Paδ, Paγ, and Paβ are apparent, as is Brackett line emission, notably in the *H*-band lines as well as Brγ in the *K*-band. There is also clear He I emission at 10 830 and 20581 Å.

(see below), this is not unexpected given the weakness of the Balmer lines.

4.1.2 Palomar 200"/TripleSpec

An infrared spectrum was taken on 2019 July 19 with the Palomar 200" telescope and facility infrared spectrograph TripleSpec (Herter et al. 2008). Similar to the DoubleSpec data, it was taken during the brightness increase of burst B5, specifically eight days earlier. The data were processed using a customized version of the `spextool` package (Cushing, Vacca & Rayner 2004), with telluric correction making use of the `xtellcorr` code (Vacca, Cushing & Rayner 2003). Fig. 2 shows the final extracted and combined spectrum, which has $R \approx 2700$.

The spectrum has a blue continuum and is relatively featureless aside from hydrogen and helium signatures. H I Brackett line emission, notably in Brγ in the *K*-band and in the higher lines above Br13 in the *H*-band, as well as Paschen line emission at Pa β, Pa γ, and Pa δ in the *J*-band is apparent. The Paschen lines appear to have some structure, perhaps a mix of absorption and emission. The Brackett pattern has the peak emission strength at Br13 and Br14, with weaker lines above and below, indicating high optical depth. Several He I emission lines are present throughout the spectral range, but there is no He II. No metal lines can be

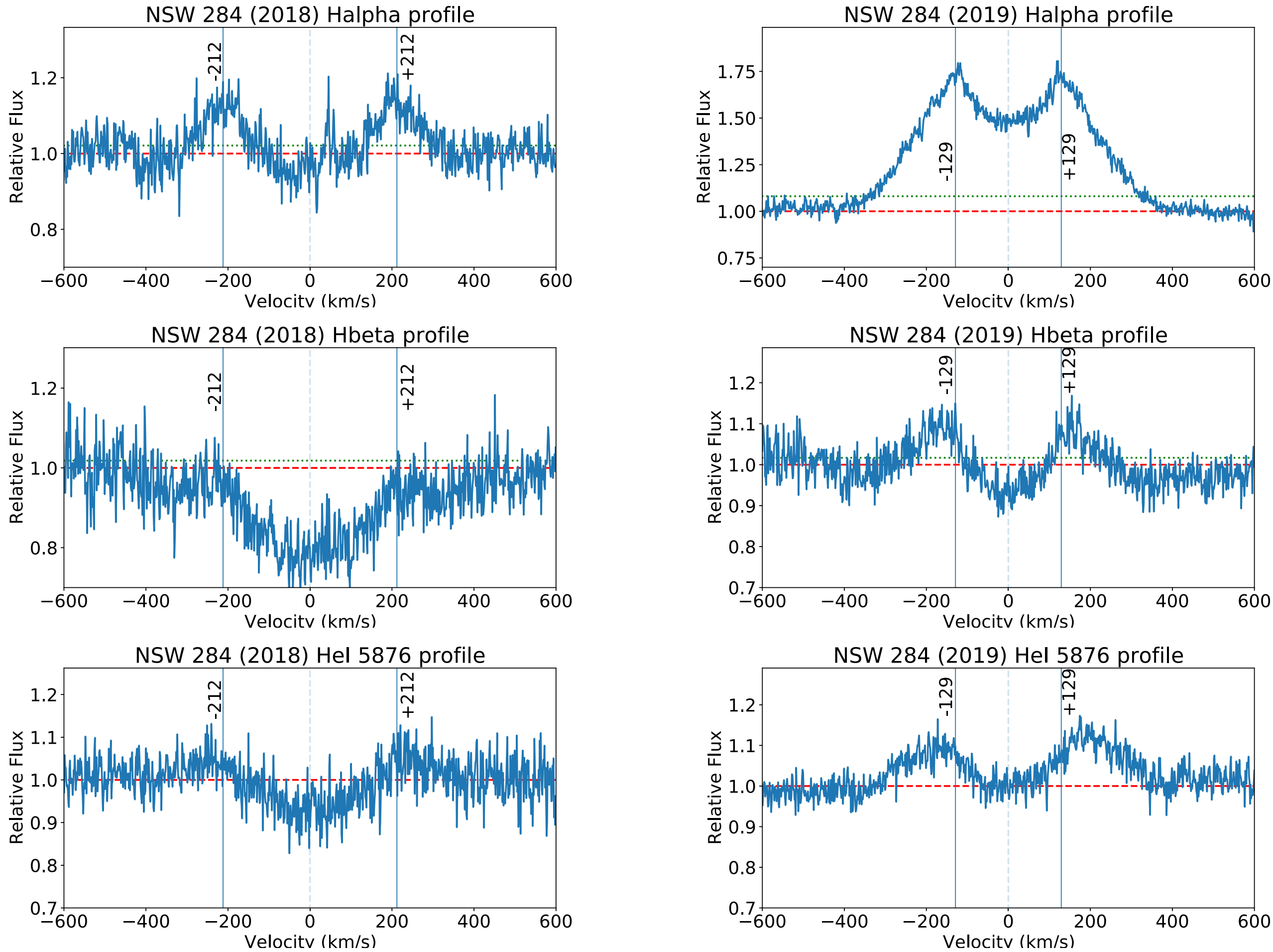

Figure 3. H α, H β, and He I 5876 Å profiles for NSW 284 from 2018 (left-hand panelss, quiescence just after weak burst B4) and 2019 (right-hand panels, during brightness decline of strong burst B5). The red dashed line shows the profile normalization level while the green dotted line indicates the 10 per cent intensity. The vertical dashed line indicates zero stellocentric velocity, adopting a heliocentric radial velocity of -57.8 km s^{-1}. Vertical lines at ± 212 km s^{-1} in 2018 and ± 129 km s^{-1} in 2019 correspond to the peaks of the double-horned profile in H α. Note that the brighter photometric state corresponds to stronger lines but lower velocities. Note also that the peaks in H β seem to be at larger velocities than the peaks in H α, and those in He I 5876 Å larger still.

identified, such as those exhibited by some Be stars (Cochetti et al. 2022).

4.1.3 *Keck/HIRES*

Two high dispersion optical spectra were obtained using the W.M. Keck Observatory and HIRES (Vogt et al. 1994) with wavelength coverage ~4800 – 9200 Å at resolution $R = 25\,000$. The observations were obtained on 2018 November 3, and 2019 November 29 (UT) and were processed using the MAKEE reduction pipeline[5] written by T. Barlow. Unfortunately, neither of the high-dispersion observations occurred during the peak of a photometric burst of NSW 284. The first spectrum was obtained in a clearly quiescent period of the light curve, just after the weak burst B4. The second spectrum has been taken during the tail end of the 2019 burst B5, where the brightness in all filters is still clearly increased compared to the base level.

The spectra are fairly featureless, with hydrogen and helium the only stellar lines. The few absorption lines that are present are broad, and indicate rapid rotation. Between the two epochs, there is a change in the presentation of these features. Velocity profiles of the H α and H β Balmer lines are illustrated in Fig. 3.

In 2018 there was weak, doubled emission apparent at H α and H β, and similarly weak and broad Paschen lines apparent starting at 8865 Å. In absorption, there are notable strong DIB features at 5488, 5491, 5508, 5780, 5797, and 6614 Å. The only stellar absorption lines are from He I (4921 Å with $W_\lambda = 0.93$ Å; 5015 Å with $W_\lambda = 0.32$ Å; 5876 Å with $W_\lambda = 0.57$ Å; and 6678 Å with $W_\lambda = 0.55$ Å). There is no He II apparent. Using the equivalent width correlations to spectral type in Leone & Lanzafame (1998), a B3 – B4 spectral type is inferred. Relevant to our analysis below, this implies a temperature for the star of $T_{\mathrm{eff}} \approx 17\,500$ K. We note that the disc emission potentially could 'fill in' the lines, and that the He I to H β line ratio is indicative of temperatures in excess of 20 000 K. This is in line with the hotter temperature of 22 666 K reported in Gaia DR3 (see Table 1), which would correspond to a spectral type ~B1. In the table we can also see that *Gaia* estimates a temperature of 15 415 K for Gaia 19eyy, which however, has almost the same absolute magnitude, extinction, and optical colours as NSW 284. It is thus not clear either how accurate the *Gaia* effective temperature estimates for these type of objects are. We thus use the estimated 17 500 K for NSW 284 (and in turn Gaia 19eyy) in our modelling later on. But we note

[5] https://astro.caltech.edu/~tb/makee/

that all model results are expressed in units of the assumed stellar temperature and can be easily scaled to other effective temperatures. Section 5.2 discusses in detail how the assumption of a different effective temperature influences the quantitative results.

In 2019 the hydrogen Balmer and Paschen lines are all stronger, with clear double-horn emission peaks. Several of the helium lines now also exhibit emission, with a similar double-peak structure. Only the 4921 Å line remains in absorption, though it is weaker now at just $W_\lambda = 0.67$ Å. An estimate for the stellar rotation can be estimated from the full-width half-maximum of this line, with v sini ≈ 280 $\mathrm{kms^{-1}}$.

From analysis of the hydrogen emission lines (Fig. 3), a heliocentric radial velocity of $-57.8\,\mathrm{kms^{-1}}$ is derived with an estimated error of at least $5\,\mathrm{kms^{-1}}$. For the 2019 spectrum, the velocity separation of the H α peaks is $\pm 129\,\mathrm{kms^{-1}}$, based on Gaussian fitting, while the full-width at 10 per cent intensity of the line is $719\,\mathrm{kms^{-1}}$. For H β the peaks are at $\pm 170\,\mathrm{kms^{-1}}$, 32 per cent higher velocity than the H α peaks. In the 2018 spectrum, the velocity separation of the H α peaks is $\pm 212\,\mathrm{kms^{-1}}$; the H β is hard to measure, though the peak separation again appears larger than for H α, closer to $231\,\mathrm{kms^{-1}}$. Between the two spectral epochs, the separation of the two velocity peaks clearly changes.

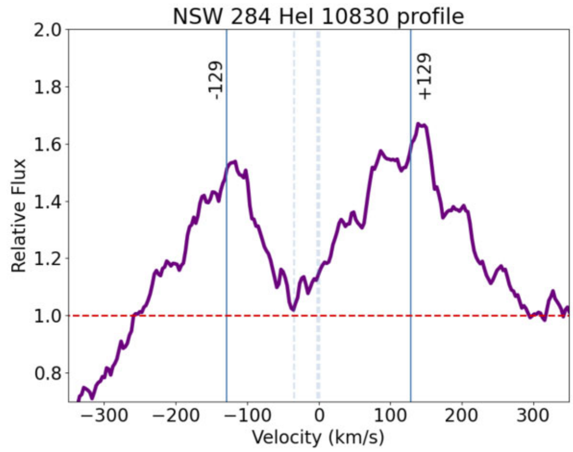

Figure 4. NIRSPEC He I 10830 Å profile of NSW 284, taken during the brightness decrease of burst B5. The three different components of the triplet line are marked at 0, −2.5, and $-34.7\,\mathrm{km\,s^{-1}}$ (dashed vertical lines). The double-horn morphology in the 10830 Å line is similar to that exhibited by the H I Balmer α and β lines, and the He I 5876 Å line (Fig. 3); the same reference velocity as for the 2019 HIRES spectrum is marked at $\pm 129\,\mathrm{km\,s^{-1}}$ (solid vertical lines).

4.1.4 Keck/NIRSPEC

Finally, a high dispersion near-infrared spectrum was obtained using the W.M. Keck Observatory and NIRSPEC (McLean et al. 1998) spectrograph covering the 1 µm Y-band at resolution $R = 19\,000$. The observations were obtained on 2019 November 17 (during the brightness decrease of burst B5) in an ABBA nodding fashion, and were processed along with a telluric standard using the REDSPEC[6] package for executing the trace, extraction, wavelength calibration, and spectral combining.

Our main interest with these observations was in the region containing the He I 10830 Å triplet line. Similar to the H I and He I lines in the optical HIRES spectrum, the He I 10830 Å is seen in double-peaked emission, with a separation between the peaks that is consistent with that in the HIRES spectrum taken at about the same time. The order also covers Pa γ. Fig. 4 shows the He I line.

4.2 VES 263

On 2019 November 29 (UT) a Keck/HIRES spectrum of VES 263 was obtained. This epoch in the light curve is a transition between bursts B10 and B11 of the source, and the first occasion where the source brightness did not fully return to the earlier baseline magnitudes. Our spectra show the Balmer lines of H α and H β with a double-horned emission profile, with the Paschen series lines exhibiting similar morphology. He I 5876 Å has a similar profile. He I 4922 Å, a hotter line, is seen in absorption with $W_\lambda = 0.21$ Å. Otherwise, the spectrum shows only a number of strong DIBS lines, specifically those at 5488, 5491 (weak), 5508 (weak), 5780, 5797, 5849, 6269, 6379, 6284, 6614 Å, plus narrow interstellar absorption in Na I D and K I.

From fitting of the hydrogen profiles (see Fig. 5) a heliocentric radial velocity of $-15.7\,\mathrm{kms^{-1}}$ is derived with an estimated error of at least $5\,\mathrm{kms^{-1}}$. However, the value of $-4.1\,\mathrm{kms^{-1}}$ reported by Munari et al. (2019) provides better centring of the double-peaked profiles, and we thus adopt that. The velocity separation of the H α peaks is $\pm 104\,\mathrm{kms^{-1}}$, based on Gaussian fitting, which can be compared to the ±130–140 $\mathrm{kms^{-1}}$ found by Munari et al. (2019). The full-width at 10 per cent intensity of the H α line is $713\,\mathrm{kms^{-1}}$. For H β the peaks are at $\pm 129\,\mathrm{kms^{-1}}$, a 24 per cent higher velocity than the H α peaks. Munari et al. (2019) have also demonstrated that the He I 5876 Å double-peaked profiles are more separated than the H α peaks at their observing epochs. They also find, similar to what we found for NSW 284, that the peak velocities change over time such that the higher velocities correspond to minimum brightness (although our interpretation of these findings differs; see our discussion below).

We do not have an infrared spectrum of VES 263, but refer the reader to fig. 4 of Munari et al. (2019). Similar to NSW 284, there is H I Paschen and Brackett line emission indicating high optical depth, as well as He I emission. The spectrum was taken during a low state, and the emission appears stronger than that in our NSW 284 high-state infrared spectrum. Additionally, there are a few metal lines that are present in emission in the infrared in VES 263.

5 INVESTIGATING THE BURST PROPERTIES

The long-term light curves in Fig. 1 and our discussion in Section 3 show that the sources have semiperiodic outbursts in brightness, with average properties reported in Table 1. The bursts repeat roughly between once or twice per year. The amplitudes and detailed shapes of each burst differ. Some bursts are very weak or absent, i.e. especially NSW 284 seems to have a quiescent period between mid-2017 and mid-2019. One feature in common among all three of our sources is that – in all bursts – the amplitudes at longer wavelengths are higher than at shorter wavelengths, and the peak brightness occurs later at longer wavelengths.

All bursts show a relatively fast increase in brightness which levels off towards the maximum brightness. The decline back towards the quiescent state is always slower than the increase. During the bursts, all colours do increase towards the peak and then return to their normal values. This clearly indicates that the additional emission from the sources during the bursts originates from material that is cooler than the surface temperature of the stars.

[6]written by L. Prato, S.S. Kim, & I.S. McLean

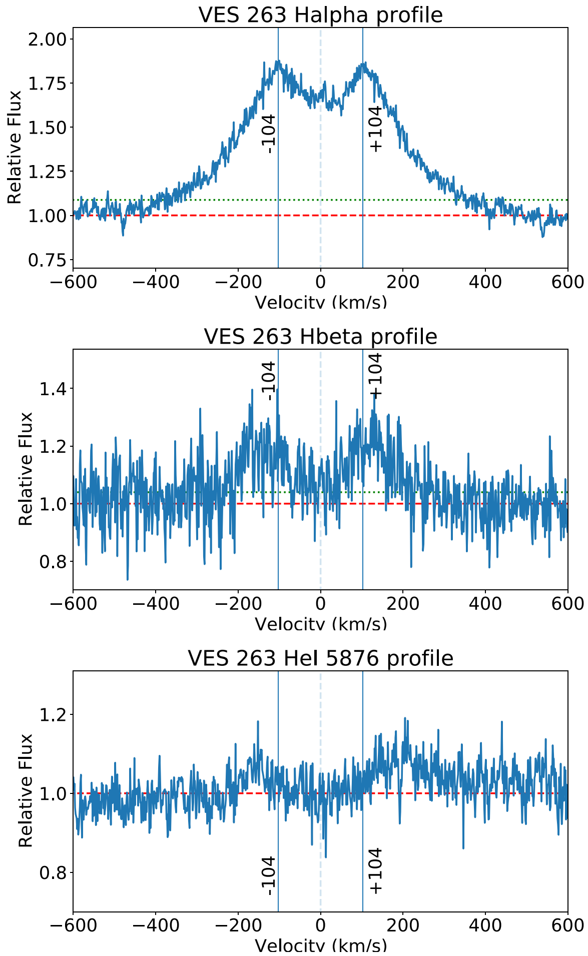

Figure 5. H α, H β, and He I 5876 Å profiles for VES 263 taken during the transition from burst B10 to B11. The horizontal red dashed line shows the profile normalization level while the green dotted line indicates the 10 per cent intensity. The vertical dashed line indicates zero stellocentric velocity, adopting a heliocentric radial velocity of -4.1 km s^{-1}. The vertical solid lines at ± 104 km s^{-1} correspond to the peaks of the double-horned profile in H α; the H β peaks have larger separation, ± 129 km/s and the He I 5876 Å larger still.

5.1 Analysis of the burst shape

All evidence is consistent with the interpretation that the objects investigated here are repeatedly outbursting Be stars. Numerical simulations and theoretical analysis of such objects by Rímulo et al. (2018, R18 hereafter) have provided an analytical description of the expected light-curve shape. The model is based on the assumption that disc loading starts at a time t_1 and continues until time t_2, when the disc material is dispersed again. According to R18 the brightness increase Δm in the light curve as a function of time t should follow the equations:

$$\Delta m = \Delta m^{\infty} \left(1 - \frac{1}{1 + [C_1 (t - t_1)]^{\eta_1}} \right) \tag{1}$$

$$\Delta m = \Delta m^{\infty} \left(1 - \frac{1}{1 + [C_1 (t_2 - t_1)]^{\eta_1}} \right) \left(\frac{1}{1 + [C_2 (t - t_2)]^{\eta_2}} \right), \tag{2}$$

where equation (1) is valid for times $t_1 \leq t \leq t_2$, and equation (2) for times $t > t_2$. The value Δm^{∞} denotes the asymptotic magnitude increase (in the filter used) that would be achieved if $t_2 - t_1$ would be very large. The parameters C and η are free parameters which depend on the filter, the source properties, and assumptions made about the disc (R18), e.g. its temperature relative to the star. The parameters differ for the brightness increase (index 1) and decrease (index 2). In particular, the C parameters depend on the viscosity α of the disc as:

$$C_1 = \alpha_1 \frac{\zeta_1}{\alpha \tau} \quad \text{and} \quad C_2 = \alpha_2 \frac{\zeta_2}{\alpha \tau}. \tag{3}$$

Following R18, the ζ and η values are determinable from numerical simulations and $\alpha\tau$ can be inferred from the intrinsic source properties as well as the orbital velocity and sound speed of the disc material according to equation (4).

$$\alpha \tau = \sqrt{\frac{R_{\rm eq}^3}{GM} \frac{v_{\rm orb}^2}{c_s^2}}. \tag{4}$$

Here $R_{\rm eq}$ is the equatorial radius of the star and M the stellar mass. The orbital velocity of the constant temperature disc is $v_{\rm orb} = (GM/R_{\rm eq})^{1/2}$, and the sound speed is determined as $c_s = \sqrt{\frac{\gamma k_B T_{\rm disc}}{\mu m_H}}$. The adiabatic index γ would be equal to 1.67 for atomic gas and the mean mass per particle $\mu = 1.3$ for typical abundances.

We have followed the description in R18 and fit the shape of all bursts for all objects using a least-squares optimization for equations (1) and (2) in all filters leaving all parameters to vary freely. We also included a part of the light-curve prior to the burst, and allowed the fitting to also determine the baseline brightness m_0 of the star, so that the observed magnitudes m in the light curve are $m = \Delta m + m_0$.

When this completely unrestricted fit was applied to the data of the same burst in different filters, it returned slightly different values for the start t_1 of the burst and the end of the disc loading t_2. It is obvious that these times should be the same for the data of the same burst in all filters. Thus, we manually chose the values for t_1 and t_2 that corresponded best to the shape of the light curve. These are typically very close to the values returned for fitting the I-band data, as this has the highest amplitude in the optical filters. These manually selected values are then fixed for all filters and other parameters are evaluated again.

The resulting fits resemble the shape of the bursts very well. We show the fit and residuals for one example burst for each source in Fig. 6. Typically the residual root mean square (RMS) of the data and fit are of the order of 0.3 – 0.4 times the photometric uncertainty for NSW 284 and Gaia 19eyy, and 0.5 – 0.6 σ for VES 263. There are some cases with small systematic deviations of the data from the fit, as e.g. during the first 30 d of the brightness increase in the burst B5 of Gaia 19eyy (see middle panel of Fig. 6). We note that the exact choice of the t_1 and t_2 values can change the best-fitting parameters (η_1, η_2, C_1, C_2). Similarly, adding or removing individual data points can cause changes in the best-fitting parameters. However, in all cases the shape of the fit and the RMS are only marginally changed. Furthermore, one can fix some of the parameters in a wide range from the best values. This causes other parameters to change without any sizeable increase in the fit RMS. For example, forcing an increase in η leads to a decrease in the corresponding C value. Thus, for the objects and bursts investigated here, fitting all free parameters in equations (1) and (2) without any constraints on η from numerical simulations, as in R18, does not allow us to investigate disc viscosity. It is beyond the scope of this paper to perform these simulations. We list our notional best-fitting parameters for all objects, bursts, and filters investigated in detail in Table A1 in the Appendix.

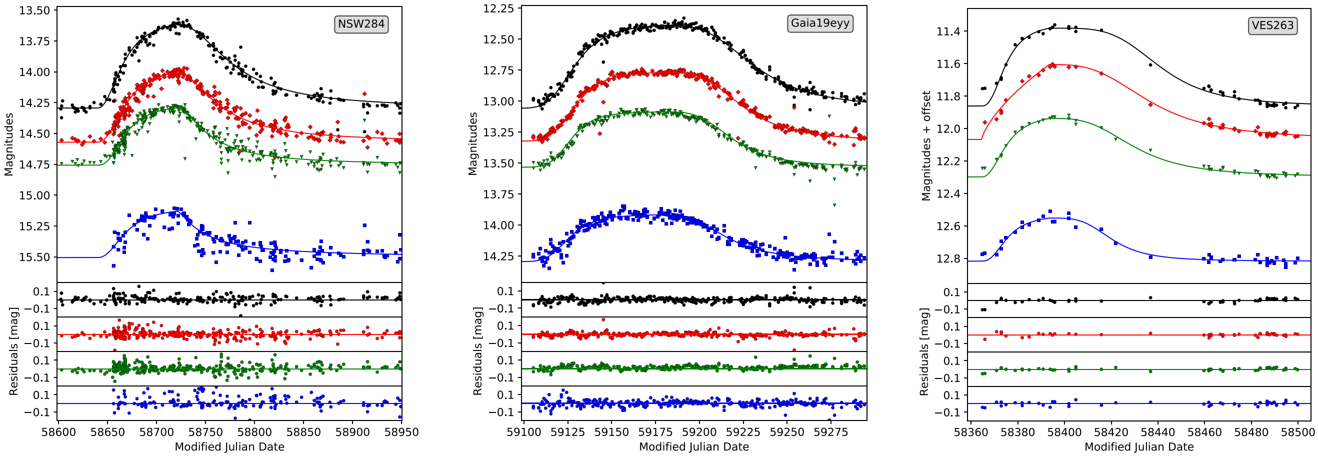

Figure 6. Detailed optical photometry and model fit for one of the bursts in each object (left-hand panel: NSW 284, Burst B5; middle: Gaia 19eyy, Burst B5; right-hand panel: VES 263, Burst B8). The symbols in the top panel show the HOYS photometry used in the light-curve fit for the different filters (from bottom to top: B – blue; V – green; R – red; I – black). The solid lines are the best fits according to equations (1) and (2). In the bottom panels we show the residuals of the data and fit with the same colour coding as in the top panel. Note that we have shifted the magnitudes of VES 263 for better visibility as follows: I: +0.8 mag, V: −0.8 mag, B: −2.1 mag.

5.2 Analysis of the burst temperature

The fits of the observed light curves in all available filters discussed in the previous section provide a smooth description of the shape of each burst. We utilize those to investigate the properties of the additional emission from the disc. This can in principle also be done with the original light-curve data, but the results would be more noisy. One obtains very similar qualitative and quantitative results for both cases. The fits hence allow us to determine the amplitudes Δm in each filter at all times after t_1. We use the PHOENIX (Husser et al. 2013) and ATLAS9 (Castelli & Kurucz 2003) stellar atmosphere models and blackbody radiation to simulate these amplitudes in our optical filters. We use the solar metallicity and $\log(g) = 4$ atmosphere models for these calculations. Note that these choices are reasonable and changing the surface gravity or metallicity only has a minimal effect on the results.

We assume that the central star has a temperature of T_S and a visible projected surface area A_S of unity. The emission responsible for the burst comes from material with a temperature T_b and a projected surface area A_b, in units of A_S. The model spectra are convolved with the filter transmission curves accessed through the astropy `PySynphot` distribution (Lim, Diaz & Laidler 2015). For each time t along the burst (in 1 d intervals), we find the burst temperature and area that result in the best-fitting (lowest RMS) amplitudes. We use a Monte Carlo approach that varies the amplitudes to fit by a standard deviation of 0.01mag – in accordance with the light-curve fit accuracy – to determine the statistical uncertainty of the best-fitting parameters. We note that our model only considers optically thick emission. The continuum emission from Be-discs is usually modelled as a combination of a pseudo-photosphere and a tenuous disc (e.g. Vieira, Carciofi & Bjorkman 2015; Vieira et al. 2017). The tenuous disc contributes typically 30 per cent of the flux via optically thin emission. Thus, we expect our model to work less well at longer wavelengths, as the optical emission will be dominated by optically thick emission based on the temperatures involved.

From the best-fitting temperature and area of the emission causing the burst, we further determine the additional luminosity of the burst based on $L_b = A_b \cdot T_b^4$ in units of the luminosity of the central star, determined the same way. Note that the choice of stellar temperature, atmospheric model spectra, and number and wavelengths of filters used only changes the resulting temperature and size evolution in a small systematic way. The qualitative behaviour does not change. Here we briefly discuss the extent to which these choices influence the quantitative results, by using burst B5 of NSW 284 as an example. The same applies to all other bursts.

We first test the influence of the choice of the stellar atmosphere model. The detailed results are shown in Fig. A1 in the Appendix. All models show the same goodness of fit (RMS). The blackbody models typically result in a luminosity that is up to 50 per cent higher compared to the PHOENIX or ATLAS models. The latter two are typically within 10 per cent of each other, with the ATLAS models predicting slightly higher luminosities. Similarly, the temperature and effective surface area of the additional emission is highest when using the blackbody models, while the two sets of model atmospheres are in agreement within the uncertainties.

As a further test, we investigate how the choice of stellar temperature in the fits influences the results. This is summarized in Fig. A3 in the Appendix. We varied the stellar temperature in steps of 1000 K between 15 500 K and 20 500 K. The first thing to note is that the quality of the fit (RMS) is completely independent of the choice of stellar temperature. Furthermore, the general qualitative behaviour of all fit parameters is not changed at all, as for all the other tests. The inferred luminosity increases by approximately 10 per cent with each 1000 K stellar temperature decrease. Similarly, the temperature of the emission decreases by the same amount. The effective size of the emitting region changes by even smaller amounts and is largest for the higher stellar temperatures. This shows that having the spectral type wrong by one sub-type (about 1000 K, more for very early B0/B1 stars), does not change the qualitative behaviour and only marginally influences the quantitative behaviour. This is especially important for Gaia 19eyy, where we have no spectra available. We note that our tested temperature range does not extend all the way to the potential value for NSW 284 from Gaia DR3 (see the discussion in Section 4.1.3). However, the qualitative results for the disc properties are unaffected and the quantitative values can be scaled to any stellar temperature chosen as discussed.

As can be seen in Fig. 1, for most bursts we have optical V, R, and I-band data. The additional B and J-band data is available only

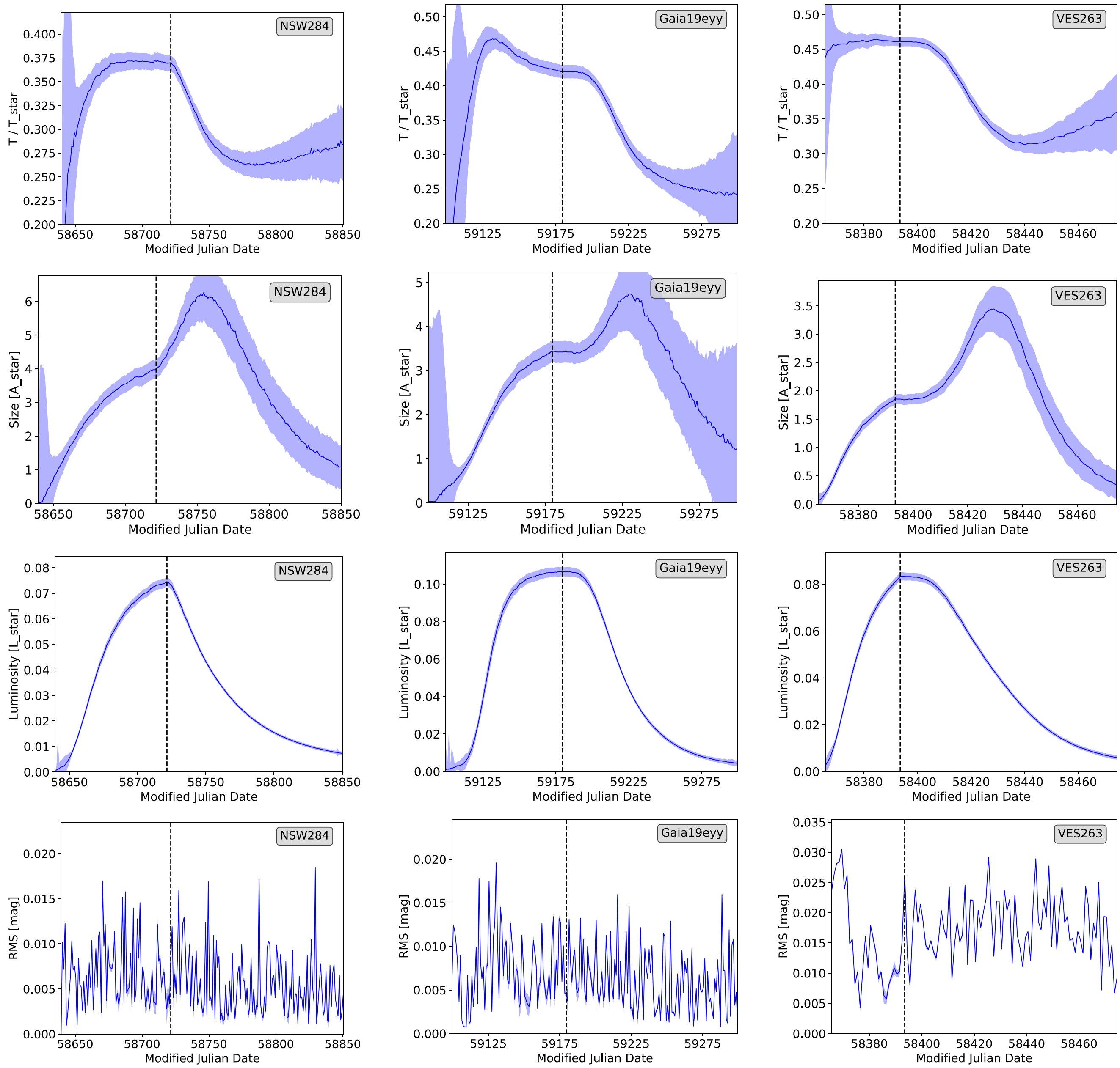

Figure 7. Example plots for the burst modelling from fitted data with template spectra (left-hand panels: NSW 284, Burst B5; middle: Gaia 19eyy, Burst B5; right-hand panels: VES 263, Burst B8). We show the temperature (1st row), size (2nd row), resulting luminosity ($L = A \cdot T^4$; 3rd row) of the additional emitting area in units of the central star and the RMS (4th row) of the fit to the light curve. The central star has been assumed to have an effective temperature of 17 500 K for NSW 284 and Gaia 19eyy and 20 500 K for VES 263. We show the fit results using the *VRI* filters for NSW 284 and Gaia 19eyy and *BVRI* for the hotter object VES 263, and using the PHOENIX models. The dashed line indicates t_2. The values for all fit parameters for each burst in all sources are listed in Table A1 in the Appendix.

for the later bursts, and also not for all sources. Naturally the mid-IR *WISE* data are available for very few dates. We have hence tested how well the models that are fit to the optical data, predict the infrared data. We show one example of this in Fig. 8. The figure shows the observational data for burst B5 in NSW 284 in the same colour code as in Fig. 1. We use the *V*, *R*, and *I*-band data to model the temperature and area of the additional emission. These values are then used to predict the amplitudes and light curve in all bands from *B* to the *WISE* filters. These predicted light curves are over plotted in Fig. 8 as solid lines.

As one would expect, all optical magnitudes, including the *B*-band which was not used in the fit, are in very good agreement with the data. The shape of the *J*-band light curve is qualitatively in good agreement with the data. However, the measured brightness values are systematically 10–20 per cent lower than the model predictions. We used the 2MASS *J*-band filter curve for the model, which is very close to the Gattini-IR filter.[7] Thus, at most only a

[7]Roger Smith; private communication

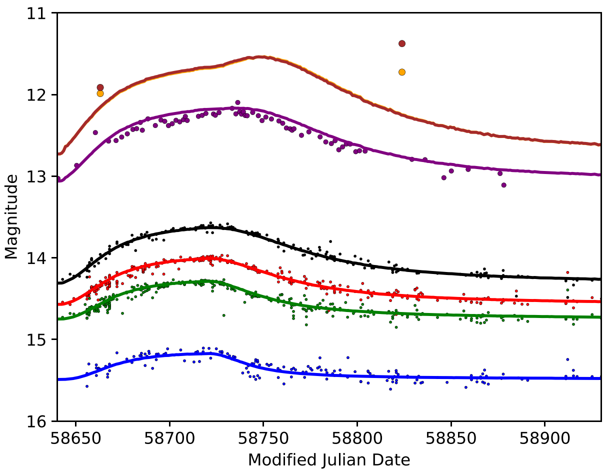

Figure 8. Data for the burst B5 of NSW 284 for the optical *B*, *V*, *R*, *I*, *J*, and *W*1/*W*2 filters (bottom to top) using the same colour codes as in Fig. 1. We over plot as solid lines the predicted amplitudes in all filters based on the fit discussed in Section 5.2 which was derived using only the observed *V*, *R*, and *I*-band data (green, red, black). Nevertheless, the *B*-band and *J*-band photometry are well-matched. The 3.6 and 4.5 µm *WISE* observations are underpredicted, however, suggesting additional emission perhaps from a free–free component of the warm gas.

very small fraction of the difference can be attributed to a difference in filter transmission curve. Furthermore, the *WISE* data points are much brighter than the predictions from the model, by up to half a magnitude. These differences, in particular the underprediction of the *WISE* data points, indicate that our simple assumption of thermal, optically thick emission from the disc to explain the bursts is not entirely correct. At the longer wavelength, additional flux from other mechanisms is significantly contributing to the bursts. This is most likely caused by free–free or synchrotron emission from the warm disc material. A set of spectra covering the optical to mid-IR wavelength range over the entire burst duration will be able to verify the nature of the emission, in combination with the above discussed models including optically thin emission from a tenuous disc (Haubois et al. 2012; Vieira et al. 2015, 2016). Our sources are ideal for such an investigation, as they show bursts at predictable intervals.

6 DISCUSSION

6.1 Summary of bursting behaviour

The three repeating Be star bursters investigated here share a number of commonalities. They all show semiregular bursts that recur once or twice per year and last for months. The typical time gaps between consecutive bursts vary for the same source by about one quarter to one-third of the average gap but vary from source to source. There are indications that the gaps between bursts slightly decrease over time, but only in VES 263 do we find a significant change in behaviour. In this object also the amplitudes of the bursts change. This suggests a change from a (photometrically) disc-less interburst phase to a long-term brightness increase, indicating a slowly growing disc in size and density. The absence of any clear periodicity excludes any burst trigger mechanism caused by binary companions. Furthermore, with the exception of VES 263, there is no discernible pattern to the amplitudes and duration of the bursts, but in all cases the rise time $t_2 - t_1$ is faster than the brightness decline back to the quiescence level after t_2. Most consistently the bursts have amplitudes that increase with wavelength. The spectra of our sources show double-peaked symmetric emission that increases in strength during the photometric bursts.

6.2 Evolution of individual bursts

When fitting the burst photometry with our simplified model, all individual bursts follow a similar pattern (if the photometric signal-to-noise is large enough). We refer the reader to Fig. 7 in what follows. The size of the emitting region in the disc increases from t_1 to t_2 while the temperatures remain roughly constant. There are some cases where the temperatures start high, but typically the SNR is too low for this to be significant. Temperatures of the disc are of the order of 0.4 times the stellar temperature, when using the adopted values for T_S in Table 2. This of course changes slightly if one uses a different stellar temperature, atmosphere model, or includes amplitudes measured at different wavelengths. However, for the most likely correct stellar temperatures, our value for the disc temperature during the burst is consistently below the 0.6 times the stellar temperature used in R18.

After the end of the mass loading at t_2, the disc temperature starts dropping in all cases. Similarly, the luminosity also peaks at this point. The disc temperature drop can be followed until the photometry SNR gets too low. The indications are that towards the end of the brightness decline, the disc temperature levels off at about a quarter to one-third of the stellar temperature. In all cases the emitting area increases from zero at t_1 to larger values at t_2. The values reached depend on the burst amplitude. After the time t_2 the best model solutions in all cases show a further increase of the emitting area. The peak is then reached at roughly the point where the decreasing disc temperature starts to level off. Following that, the emitting area shrinks until the end of the burst to effectively zero in all cases. If our model is correct, this would indicate that after mass loading stops, the main emitting area of the disc gets pushed away from the star. This expands the emitting area and cools the material, before the radial thickness of the emitting area in the disc shrinks. There are some simulations of the radial disc density profile during bursts roughly similar to our scenario (e.g. top panel of fig. 7 in Haubois et al. 2012). However, they do not show the evolution after the mass loading stops and we are thus not able to compare them directly to our observations.

The rate of increase of the burst luminosity at the point t_2 shows that the end of the mass loading occurs at different parts of the burst. In the majority of the cases the luminosity increase just prior to t_2 is still very steep or has just started to level off. In some cases, most notable for burst B5 in Gaia 19eyy, the luminosity has plateaued before t_2 is reached. This shows that whatever mechanism stops the mass loading process can occur at any time after t_1. Since only very few of the bursts reach a stable, steady-state luminosity and the gap between bursts is much longer than the rise time, the trigger mechanism to stop the mass loading must occur much more frequently than the trigger to start the mass loading process. This is further emphasized by the occasional very weak burst, e.g. in NSW 284, where the mass loading most likely stops immediately after it has been triggered.

The fit to the amplitudes using equations (1) and (2) results in all cases in an RMS that is smaller than the typical photometric uncertainties of the individual brightness measurements.[8] This is

[8]There are some minor exceptions such as the start of the burst B5 in Gaia 19eyy.

strong evidence that the theoretical framework in R18 correctly predicts the shape of the bursts. The accuracy by which the model fits the optical and even the unconstrained near infrared amplitudes (see Fig. 8), further justifies this approach. Furthermore, the high optical depth inferred from our NIR spectrum of NSW 284 (Section 4.1.2) also supports our attempt at modelling the burst continuum emission with stellar atmosphere or blackbody models.

The comparison of the spectra taken in quiescence and burst show that emission does not just increase in brightness. The peak emission also moves to lower velocities, i.e. happens further out in the disc. This fits well with the decretion disc model. Our photometry modelling further supports this picture, indicating cooling, expansion, and probably radial outward drift of the main emitting part of the disc after t_2. Using the measured velocities and modelled emitting surface area, one finds that the main emission is confined to a narrow ring with a radial thickness of the order of 0.5 to one solar radius.

6.3 Uncertain physical parameters

Despite the apparent successes in matching a heuristic model to optical light-curve data, it is clear that there are limitations to our simplified model.

First, it is not possible to fit accurately all the parameters in these equations at the same time. Thus, it is not possible to investigate the viscosity of the discs without additional assumptions or simulations as in R18, Haubois et al. (2012) or Carciofi et al. (2012).

Secondly, the model considers only a single temperature disc rather than a small Keplerian disc. We have seen from the high resolution spectra (Section 4) that the peaks of the double-horned line profiles are at higher velocities for higher excitation transitions. Thus, there are clear indications of a radial temperature gradient in the disc during the burst, and presumably as well in quiescence. This could explain the 10 – 20 per cent overprediction of the *J*-band magnitudes.

Our model furthermore does not use any real radiative transfer. It thus will not be able to handle any outbursting Be stars where we observe the disc edge-on, which usually results in brightness dips at the shorter wavelengths. For the MIR data the model underpredicts the observed amplitudes in the *WISE* filters by up to half a magnitude. This strong MIR excess emission compared to our optically thick emission model indicates significant contribution from free–free emission in these Be discs. This is in line with previous works showing that typical Be stars have infrared access governed by free–free emission (Finkenzeller & Mundt 1984).

6.4 VES 263 in context

VES 263 is the only one of our sources that has been studied in any detail previously. Munari et al. (2019, in section 8) interpret their data for this object in terms of Herbig Ae/Be star accretion, but we take the photometric and spectroscopic evidence as indicative of a decretion disc, with gas flowing outwards rather than inwards.

Munari et al. (2019) also model the SED of VES 263 during quiescence and burst. They fit quiescence to a 20 000 K template, and add blackbody emission at 4500 and 7500 K for the two different brighter phases. This can be compared to the approximately 9000 K disc temperature inferred from our light-curve fit here. As one can see from Fig. 7, we find that during the burst the luminosity increases by up to 8 per cent. This equates to roughly 1000 $L_\odot$, which is in line with the sum of the two additional luminosities (120 + 860 $L_\odot$) inferred by Munari et al. (2019). Note that the Munari et al. (2019) model also includes, in the quiescent state, a dust continuum excess fit to two AKARI data points, that is a blackbody disc with maximum temperature of 400 K and luminosity of 12 $L_\odot$. This emission is most likely always present, but becomes insignificant during the bursts.

The presence of cold dust does not necessarily rule out our interpretation of the nature of this source. Dust has been shown to form in many other hot environments, such as e.g. novae (Derdzinski, Metzger & Lazzati 2017) or Wolf–Rayet binaries (Usov 1991). In those cases dust formation episodes can occur in dense shocks formed due to the interaction of outflowing material or winds with circumstellar material. While outflow velocities and densities need to be high for this, this mechanism remains a possible source for dust formation in VES 263.

6.5 The broader context

The objects investigated here provide textbook examples of regularly outbursting Be stars. Indeed there are very few really regularly outbursting Be stars known. A short list is presented in Baade et al. (2017) and a handful are listed in Labadie-Bartz et al. (2022). But these objects vary on shorter time-scales (up to tens of days) between bursts and at most a few per cent amplitudes. Semiregular variations are much more common (e.g. Labadie-Bartz et al. 2017). However, typically these objects show a much larger variation of the times between bursts, large burst to burst amplitude variations, slightly smaller amplitudes than the objects discussed here, and the bursts do not follow the general shape from equations (1) and (2). Thus, the sources discussed here, represent rare cases of truly regularly outbursting Be stars.

While we have been able to piece together light curves from several different long-term photometric surveys, the spectroscopic coverage is less than desirable. For example, we do not have time-series high resolution spectra available at multiple stages of any of the bursts. This would enable us to study in detail the temperature and radial evolution of the emitting disc material during the burst. Additionally valuable observations would be *JHK* spectroscopic monitoring throughout a burst. This would enable the modelling of the thermal and non-thermal contributions to the spectrum as the burst evolves. However, because the timing of the bursts can be predicted in advance – in most cases within a few weeks – future observations can be planned.

We also note that there are other likely outbursting Be objects that are being revealed through ongoing time domain surveys, but remain poorly studied. We have identified the following potentially similar objects to those we have studied, based on their public light curves: Gaia22bre[9], Gaia22axt[10], ASASSN-V J210822.32+584613.4[11], and potentially AP565575.[12] Again, spectroscopic follow-up is warranted.

Considering the larger population of early-type stars, we note that the vast majority of OB-type stars are binaries (Moe & Di Stefano 2017). There are no clear indications in any of our spectra that the sources we have investigated are binaries. There are no general radial velocity shifts between spectra taken at different times. The disc emission profiles furthermore, rule out any close, low mass companion, which would disturb the disc. As discussed above, the non-periodic nature of the bursts excludes the presence of highly elliptical companions with small perihelion distances. We

[9] http://gsaweb.ast.cam.ac.uk/alerts/alert/Gaia22bre/
[10] http://gsaweb.ast.cam.ac.uk/alerts/alert/Gaia22axt/
[11] https://asas-sn.osu.edu/variables/587872
[12] https://asas-sn.osu.edu/photometry/f5962fee-2400-55ba-b692-4946613cf59a

cannot rule out any wide, lower mass companions with the data available. The spectral energy distributions give no indication of a second component. The above suggested high resolution time-series spectroscopy could provide more stringent constraints on the multiplicity of the sources.

Returning to the viscous decretion disc model described in the introduction, our observations and modelling support a general picture in which Be star outbursts correspond to a rapid temperature rise in the discs over an initially small area, and a gradual increase in the total area participating in the higher temperatures.

7 CONCLUSIONS

We collected long-term optical photometric data for the three variable sources NSW 284, Gaia19eyy, and VES 263. These are supplemented by NIR and NEO-WISE photometry, and high resolution spectra. We characterize these sources as rare cases of truly regularly outbursting Be stars.

The bursts in these sources occur semiregularly with a cadence between half to one year and a duration from about 120 to 200 d. The burst amplitudes are variable and reach a maximum of about half a magnitude in the *R*-band. In all cases the amplitudes increase towards longer wavelengths, and the peak of the bursts shifts to later times at longer wavelengths.

We fit the individual burst light curves with the theoretical burst shape model from Rímulo et al. (2018). This provides an excellent fit to the data in all cases. The typical RMS of the fit is of the order or better than half the photometric uncertainty in the data. However, despite this excellent fit, the fit parameters cannot be constrained accurately as they depend on each other. Thus, in order to study e.g. the disc viscosity during and after mass loading, the photometry needs to be supplemented by numerical simulations, as performed by Rímulo et al. (2018).

The burst shapes in all cases show a steep increase in brightness and a longer lasting fall back. The duration of the brightness increase represents the typical duration between a (mass loading) burst trigger event and the trigger that stops the mass loading. This duration (50 – 80 d) is always much shorter than separation of consecutive bursts (120 – 200 d). Thus, the trigger that stops the mass loading occurs on average 3 – 5 times more frequent than the trigger that starts the mass loading. Thus, any physical explanation for the occurrence of these bursts and their end will have to account for this. In some cases, the bursts stop almost immediately after their start, leading to very low amplitudes or even undetected bursts, e.g. the '?' and B4 bursts in NSW 284.

We model the smoothed burst light curves with a simple model that attempts to reproduce the amplitude increase in the different filters over time with a simple single temperature emitter surrounding the host star. The host star and additional emitter are modelled with different template atmospheric spectra or blackbody emission. The models predict the size (relative to the host star) and temperature of the additional emitter during the burst. The resulting values for those are only marginally (quantitatively) influenced by the exact value of the stellar surface temperature chosen – which is not known exactly. The qualitative behaviour of size and temperature evolution of the additional emitter during the burst is always well constrained. In particular, we find that the surface temperature of the additional emitter is of the order of 40 per cent of the stellar temperature. This is lower than the 60 per cent assumed in the work by Rímulo et al. (2018). Our simple model underpredicts the observed amplitudes in the *WISE* filters by up to half a magnitude, indicating a significant contribution from free–free emission in these Be discs.

All three sources investigated in this work show very regular and predictable burst behaviour, albeit with unpredictable variations in amplitude, over the better part of a decade. They thus present excellent candidates for follow up high cadence spectroscopy and photometry of their future bursts. This would allow more detailed models of the outbursting Be phenomenon to be developed to identify, in particular, the triggering mechanism for the start and the stop of the disc mass loading process in these sources.

A notable aspect of our sample is that two of the three objects studied here have been previously discussed in the literature as young Herbig Ae/Be stars, rather than as evolved Be stars. It is thus worth emphasizing the value of long-term light curves, such as those produced by the HOYS survey and other long-term photometric surveys such as ASAS-SN and PTF/ZTF.

DATA AVAILABILITY STATEMENT

Some of the photometry data underlying this article are available in the HOYS data base at http://astro.kent.ac.uk/HOYS-CAPS/. Some of the spectroscopic data are available in the Keck Observatory Archive (KOA).

ACKNOWLEDGEMENTS

Our referee is acknowledged for a helpful report. We would like to thank all contributors of optical photometric data for their efforts towards the success of the HOYS project. We also thank the entire Gattini-IR team for access to infrared photometry of our sources. We acknowledge Tony Rodriguez for assistance in acquiring and reducing the Palomar/DoubleSpec data for NSW 284 that is reported here, and Adolfo Carvalho for assistance with DIBs feature identification in the HIRES spectra. JCW was funded by the European Union (ERC – European Research Council, 101039452). This work has made use of data from the European Space Agency (ESA) mission *Gaia* (https://www.cosmos.esa.int/gaia), processed by the *Gaia* Data Processing and Analysis Consortium (DPAC, https://www.cosmos.esa.int/web/gaia/dpac/consortium). Funding for the DPAC has been provided by national institutions, in particular the institutions participating in the *Gaia* Multilateral Agreement. All authors from Silesian University of Technology were responsible for data processing and automation of observations at SUTO observatories and were financed by grant BK-246/RAu-11/2022. Piotr Jóźwik-Wabik also acknowledges support from grant BKM-574/RAu-11/2022 and 32/014/SDU/10-22-20.

DATA AVAILABILITY STATEMENT

Some of the photometry data underlying this article are available in the HOYS data base at http://astro.kent.ac.uk/HOYS-CAPS/. Some of the spectroscopic data are available in the Keck Observatory Archive (KOA).

REFERENCES

Baade D., Rivinius T., Pigulski A., Carciofi A., BEST Collaboration, 2017, in Miroshnichenko A., Zharikov S., Korčáková D., Wolf M.eds, ASP Conf. Ser. Vol. 508, The B[e] Phenomenon: Forty Years of Studies. Astron. Soc. Pac., San Francisco, p. 93

Bellm E. C. et al., 2019, PASP, 131, 018002

Berlanas S. R., Wright N. J., Herrero A., Drew J. E., Lennon D. J., 2019, MNRAS, 484, 1838

Bernhard K., Otero S., Hümmerich S., Kaltcheva N., Paunzen E., Bohlsen T., 2018, MNRAS, 479, 2909
Carciofi A. C., Bjorkman J. E., Otero S. A., Okazaki A. T., Štefl S., Rivinius T., Baade D., Haubois X., 2012, ApJ, 744, L15
Carvalho A. S., Hillenbrand L. A., 2022, ApJ, 940, 156
Castelli F., Kurucz R. L., 2003, in Piskunov N., Weiss W. W., Gray D. F.eds, Proc. IAU Symp. 210, Modelling of Stellar Atmospheres. Cambridge Univ. Press, Cambridge, p. A20
Chojnowski S. D. et al., 2015, AJ, 149, 7
Cochetti Y. R., Arias M. L., Cidale L. S., Granada A., Torres A. F., 2022, A&A, 665, A115
Comerón F., Pasquali A., 2012, A&A, 543, A101
Cushing M. C., Vacca W. D., Rayner J. T., 2004, PASP, 116, 362
Cutri R. M. et al., 2012, VizieR Online Data Catalog, p. II/311
Cutri R. M. et al., 2021, VizieR Online Data Catalog, p. II/328
De K. et al., 2020, PASP, 132, 025001
Derdzinski A. M., Metzger B. D., Lazzati D., 2017, MNRAS, 469, 1314
Drew J. E. et al., 2005, MNRAS, 362, 753
Evitts J. J. et al., 2020, MNRAS, 493, 184
Finkenzeller U., Mundt R., 1984, A&AS, 55, 109
Froebrich D. et al., 2018, MNRAS, 478, 5091
Gaia Collaboration, 2016, A&A, 595, A1
Gaia Collaboration, 2022, VizieR Online Data Catalog, p. I/355
Ghoreyshi M. R. et al., 2018, MNRAS, 479, 2214
Hambsch F. J., 2012, J. Am. Assoc. Var. Star Obs., 40, 1003
Haubois X., Carciofi A. C., Rivinius T., Okazaki A. T., Bjorkman J. E., 2012, ApJ, 756, 156
Herter T. L. et al., 2008, in McLean I. S., Casali M. M.eds, Proc. SPIE Conf. Ser. Vol. 7014, Ground-based and Airborne Instrumentation for Astronomy II. SPIE, Bellingham, p. 70140X
Hodgkin S. T. et al., 2021, A&A, 652, A76
Husser T. O., Wende-von Berg S., Dreizler S., Homeier D., Reiners A., Barman T., Hauschildt P. H., 2013, A&A, 553, A6
Kochanek C. S. et al., 2017, PASP, 129, 104502
Kohoutek L., Wehmeyer R., 1997, Astron. Abh. Hamburger Sternwarte, 11, 1
Labadie-Bartz J. et al., 2017, AJ, 153, 252
Labadie-Bartz J. et al., 2018, AJ, 155, 53
Labadie-Bartz J., Carciofi A. C., Henrique de Amorim T., Rubio A., Luiz Figueiredo A., Ticiani dos Santos P., Thomson-Paressant K., 2022, AJ, 163, 226
Law N. M. et al., 2009, PASP, 121, 1395
Lee U., Osaki Y., Saio H., 1991, MNRAS, 250, 432
Leone F., Lanzafame A. C., 1998, A&A, 330, 306
Lim P. L., Diaz R. I., Laidler V., 2015, Astrophysics Source Code Library, record ascl:1303.023
Mainzer A. et al., 2011, ApJ, 731, 53
Masci F. J. et al., 2019, PASP, 131, 018003
McLean I. S. et al., 1998, in Fowler A. M.ed., Proc. SPIE Conf. Ser. Vol. 3354, Infrared Astronomical Instrumentation. SPIE, Bellingham, p. 566
Mennickent R. E., Pietrzyński G., Gieren W., Szewczyk O., 2002, A&A, 393, 887
Moe M., Di Stefano R., 2017, ApJS, 230, 15
Moore A. M., Kasliwal M. M., 2019, Nat. Astron., 3, 109
Munari U. et al., 2019, MNRAS, 488, 5536
Nakano M., Sugitani K., Watanabe M., Fukuda N., Ishihara D., Ueno M., 2012, AJ, 143, 61
Neiner C., de Batz B., Cochard F., Floquet M., Mekkas A., Desnoux V., 2011, AJ, 142, 149
Oke J. B., Gunn J. E., 1982, PASP, 94, 586
Porter J. M., 1996, MNRAS, 280, L31
Ressler S. M., 2021, MNRAS, 508, 4887
Richardson N. D. et al., 2021, MNRAS, 508, 2002
Ricker G. R. et al., 2015, J. Astron. Telesc. Instrum. Syst., 1, 014003
Rímulo L. R. et al., 2018, MNRAS, 476, 3555
Rivinius T., Carciofi A. C., Martayan C., 2013, A&AR, 21, 69
Rivinius T., Baade D., Carciofi A. C., 2016, A&A, 593, A106
Semaan T., Hubert A. M., Zorec J., Gutiérrez-Soto J., Frémat Y., Martayan C., Fabregat J., Eggenberger P., 2018, A&A, 613, A70
Shappee B. J. et al., 2014, ApJ, 788, 48
Slettebak A., 1982, ApJS, 50, 55
Slettebak A., Collins George W. I., Truax R., 1992, ApJS, 81, 335
Tonry J. L. et al., 2018, PASP, 130, 064505
Usov V. V., 1991, MNRAS, 252, 49
Vacca W. D., Cushing M. C., Rayner J. T., 2003, PASP, 115, 389
Vieira R. G., Carciofi A. C., Bjorkman J. E., 2015, MNRAS, 454, 2107
Vieira R. G., Carciofi A. C., Bjorkman J. E., 2016, MNRAS, 455, 2607
Vieira R. G., Carciofi A. C., Bjorkman J. E., Rivinius T., Baade D., Rímulo L. R., 2017, MNRAS, 464, 3071
Vogt S. S. et al., 1994, in Crawford D. L., Craine E. R.eds, Proc. SPIE Conf. Ser. Vol. 2198, Instrumentation in Astronomy VIII. SPIE, Bellingham, p. 362
Wang L. et al., 2022, ApJS, 260, 35
Wright E. L. et al., 2010, AJ, 140, 1868

APPENDIX A: BEST BURST FIT PARAMETERS

When one includes the *B*-band amplitudes (which are not generally available for all bursts), there are some small systematic differences in the determined burst properties. This is shown in Fig. A2 in the Appendix. The burst temperature is slightly higher when including the *B*-amplitudes. This is of the same order as the increase seen when using the blackbody models instead of the other two, i.e. about 10 per cent. The size and luminosity also vary by this amount. The most important difference when including the *B*-amplitudes into the fit is that the RMS typically increases. In our example burst it is by almost a factor of three, from 0.007 mag to about 0.02 mag – which is still of the order of the photometry uncertainty of the data. This is most likely caused by the simplicity of our model, i.e. the assumption of a single temperature disc and all emission being thermal. The disc temperature will certainly change with distance from the star. And at the typical disc temperatures we derive, the *B*-filter covers roughly the peak of the SED. This is also notable in the individual fits shown in Fig. 7. There, one can see that the RMS can be higher at the start of the burst, during the mass loading phase compared to the decline in brightness at the end.

Table A1. Table listing the fit results from equations (1) and (2) for the bursts with sufficient HOYS data available. For each burst we list the filter, the baseline magnitude, the asymptotic magnitude increase, the manually determined start t_1 and end t_2 time of mass loading, its duration, as well as the η and C parameters.

Filter	m_0 (mag)	Δm^∞ (mag)	t_1 (MJD)	t_2 (MJD)	$t_2 - t_1$ (d)	η_1	η_2	C_1 (d^{-1})	C_2 (d^{-1})
NSW 284, burst B3									
I	14.305	−0.639	57666	57750	84	2.361	1.604	0.038	0.022
R	14.572	−0.803	57666	57750	84	1.621	1.325	0.021	0.043
V	14.772	−0.431	57666	57750	84	2.280	1.292	0.037	0.037
NSW 284, burst B5									
I	14.294	−0.740	58640	58722	82	2.191	2.047	0.037	0.017
R	14.571	−0.625	58640	58722	82	2.241	1.815	0.034	0.022
V	14.757	−0.498	58640	58722	82	2.526	1.649	0.035	0.029
B	15.506	−0.413	58640	58722	82	2.282	1.254	0.034	0.035
NSW 284, burst B6									
I	14.274	−0.723	58983	59035	52	1.378	2.061	0.034	0.029
R	14.561	−0.466	58983	59035	52	2.317	1.712	0.044	0.035
V	14.755	−0.505	58983	59035	52	1.400	1.745	0.029	0.040
B	15.481	−0.376	58983	59035	52	1.154	1.307	0.031	0.045
NSW 284, burst B8									
I	14.269	−0.666	59550	59650	100	0.984	2.577	0.023	0.020
R	14.562	−0.569	59550	59650	100	1.184	2.418	0.023	0.018
V	14.762	−0.458	59550	59650	100	0.544	1.928	0.023	0.017
Gaia 19eyy, burst B5									
I	13.057	−0.686	59095	59180	85	4.046	3.202	0.029	0.019
R	13.322	−0.563	59095	59180	85	4.590	3.398	0.029	0.022
V	13.533	−0.450	59095	59180	85	5.035	3.414	0.031	0.025
B	14.295	−0.383	59095	59180	85	4.424	2.848	0.032	0.027
Gaia 19eyy, burst B6									
I	13.020	−1.115	59507	59570	63	0.712	3.062	0.032	0.015
R	13.297	−2.576	59507	59570	63	0.615	3.432	0.003	0.014
V	13.538	−2.260	59507	59570	63	0.723	3.668	0.004	0.016
B	14.278	−0.633	59507	59570	63	1.160	2.641	0.043	0.020
VES 263, burst B8									
I	11.061	−0.519	58365	58394	29	2.471	4.193	0.095	0.021
R	12.067	−3.605	58365	58394	29	0.753	3.082	0.003	0.023
V	13.098	−0.400	58365	58394	29	2.257	3.163	0.092	0.027
B	14.917	−0.291	58365	58394	29	2.468	3.684	0.089	0.037

APPENDIX B: BURST TEMPERATURE ANALYSIS PLOTS

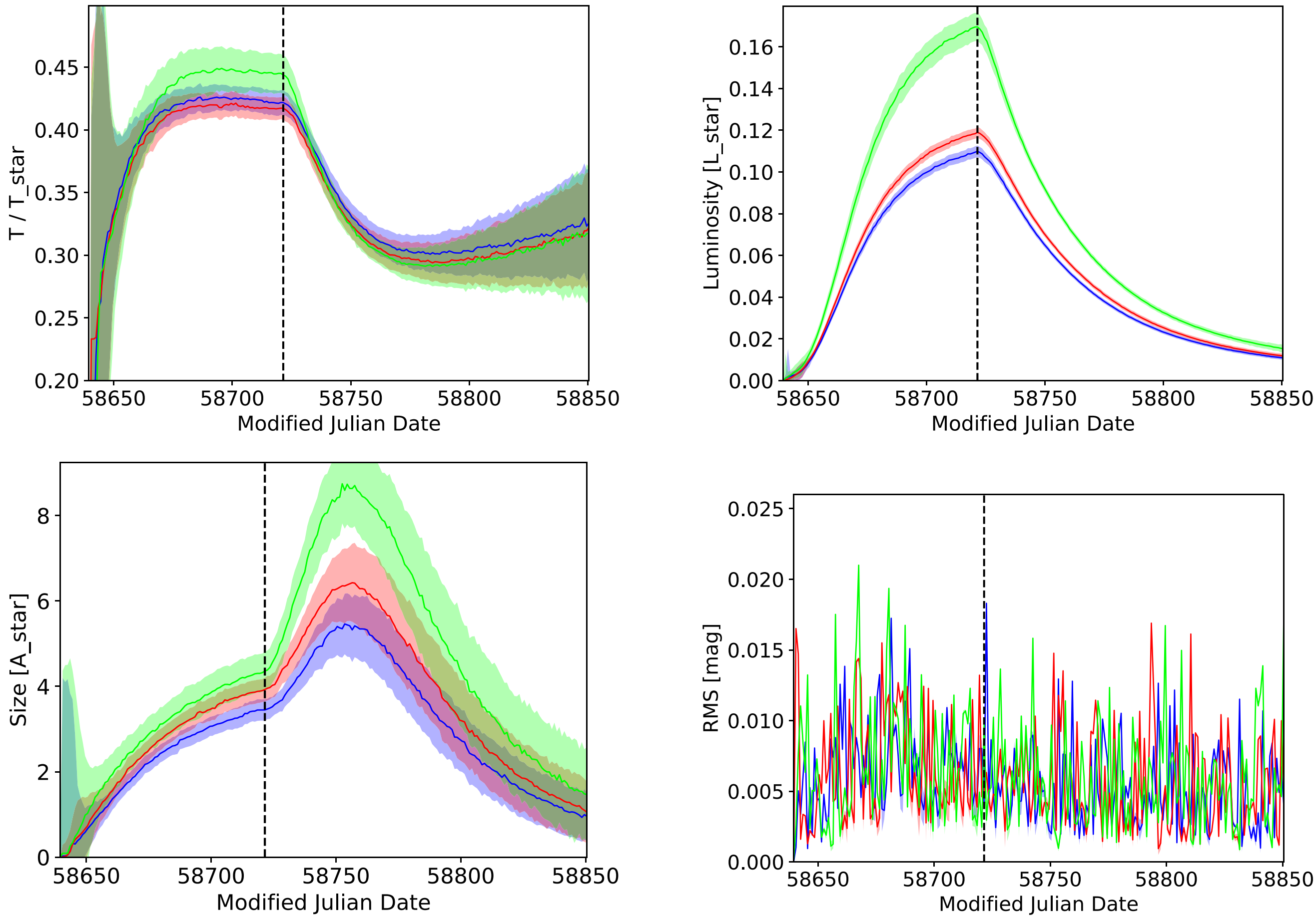

Figure A1. Example of a burst fit using different model stellar atmospheres. We show the fit to burst B5 of NSW 284, using a stellar temperature of 17 500 K and the *VRI* photometry. If applicable we use $\log(g) = 4.0$ and $[M/H] = 0.0$. The colours indicate the use of the PHOENIX (blue), ATLAS (red), and blackbody (green) stellar atmosphere models and the lightly shaded areas the uncertainties.

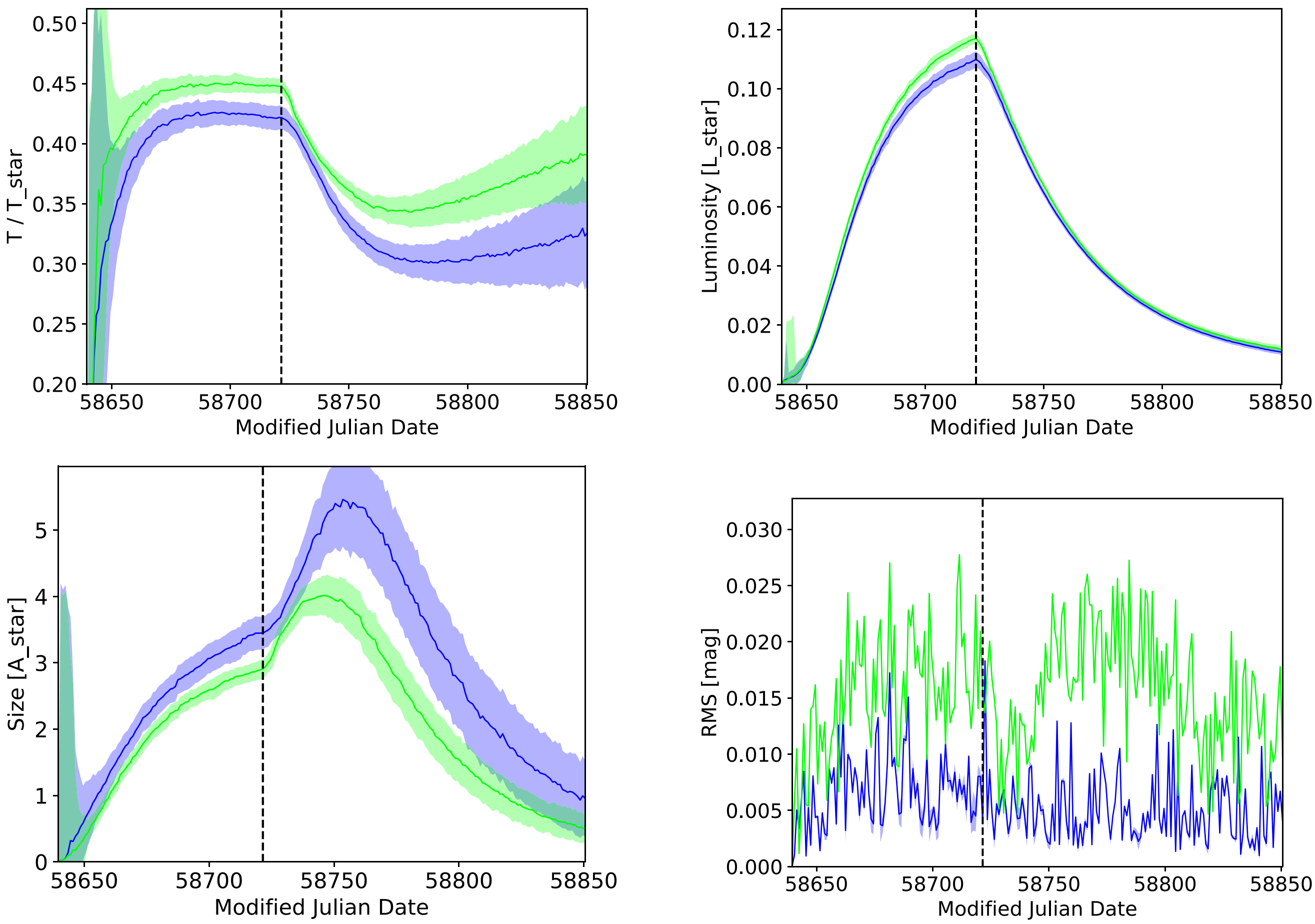

Figure A2. Example of a burst fit using different sets of filters. We show the fit to burst B5 of NSW 284, using a stellar temperature of 17 500 K and the PHOENIX stellar atmosphere models. We use $\log(g) = 4.0$ and [M/H] = 0.0. The colours indicate the use of the *VRI* amplitudes (blue) and the *BVRI* amplitudes (green) and the lightly shaded areas the uncertainties.

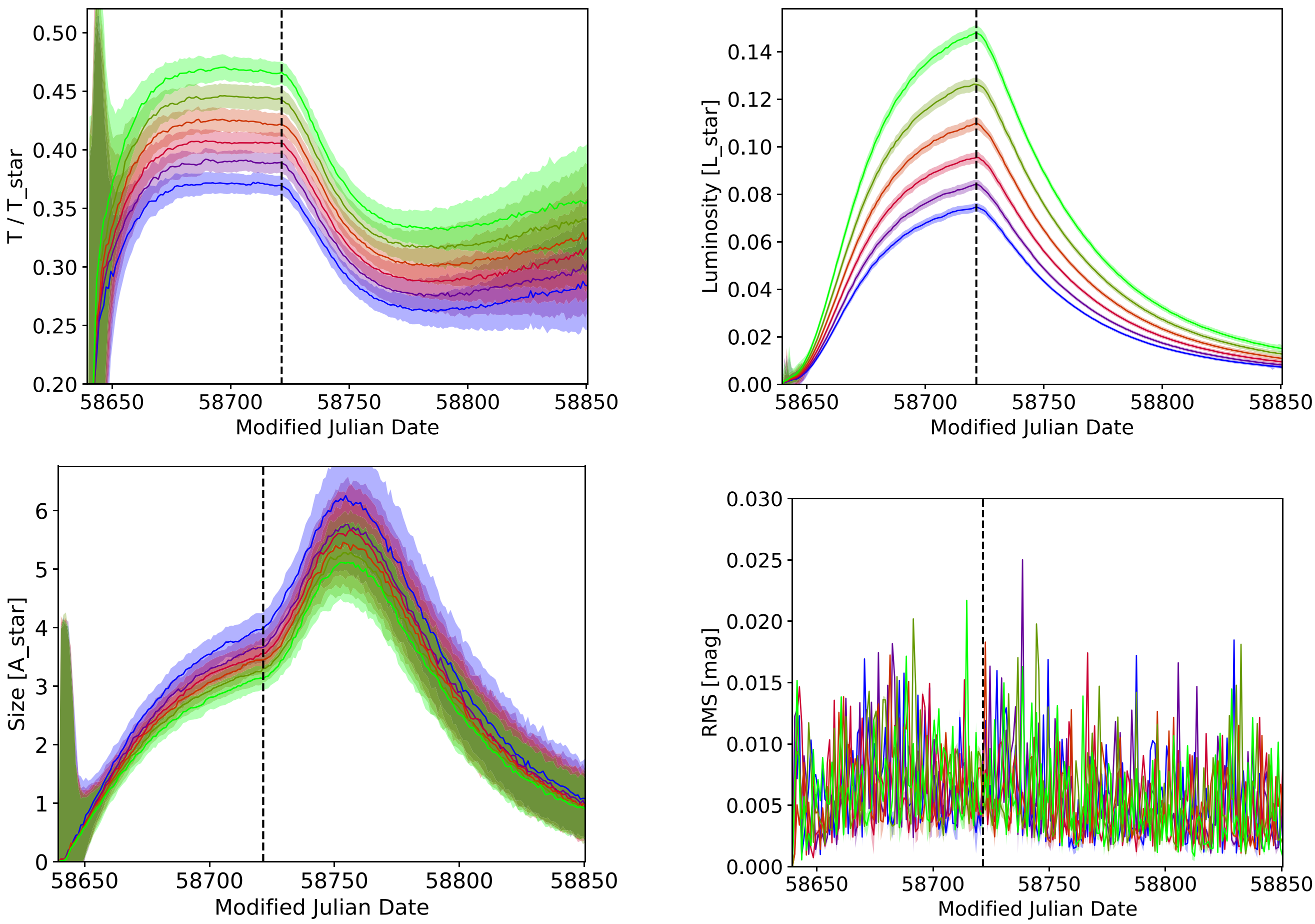

Figure A3. Example of a burst fit using different stellar temperatures. We show the fit to burst B5 of NSW 284, using the PHOENIX stellar atmosphere models and the *VRI* filters. We use log (g) = 4.0 and [M/H] = 0.0. The colours indicate the adopted stellar temperature ranging from 15 500 K (green) to 20 500 K (blue) in steps of 1000 K and the lightly shaded areas the uncertainties.

[1] *School of Physical Sciences, University of Kent, Canterbury CT2 7NH, UK*
[2] *Department of Astronomy, MC 249-17, California Institute of Technology, Pasadena, CA 91125, USA*
[3] *Centre for Astrophysics and Planetary Science, School of Physical Sciences, University of Kent, Canterbury CT2 7NH, UK*
[4] *MIT-Kavli Institute for Astrophysics and Space Research, 77 Massachusetts Ave., Cambridge, MA 02139, USA*
[5] *Thüringer Landessternwarte, Sternwarte 5, D-07778 Tautenburg, Germany*
[6] *European Southern Observatory, Karl-Schwarzschild-Straße 2, D-85748 Garching, Germany*
[7] *SUPA, School of Science and Engineering, University of Dundee, Nethergate, Dundee DD1 4HN, UK*
[8] *Vereniging voor Sterrenkunde, werkgroep veranderlijke sterren, Oostmeers 122 C, B-8000 Brugge, Belgium*
[9] *Bundesdeutsche Arbeitsgemeinschaft für Veränderliche Sterne e.V. (BAV), Munsterdamm 90, D-12169 Berlin, Germany*
[10] *AAVSO, 49 Bay State Road, Cambridge, MA 02138, USA*
[11] *The British Astronomical Association, Variable Star Section, Burlington House Piccadilly, London W1J 0DU, UK*
[12] *Department of Electronics, Electrical Engineering and Microelectronics, Silesian University of Technology, Akademicka 16, PL-44-100 Gliwice, Poland*
[13] *Public Observatory AstroLAB IRIS, Provinciaal Domein De Palingbeek, Verbrandemolenstraat 5, B-8902 Zillebeke, Ieper, Belgium*
[14] *Astronomical Society of Edinburgh, Edinburgh, UK*
[15] *Observadores de Supernovas, Spain*
[16] *Uraniborg Observatory, Calle Antequera 8, Écija, E-41400 Sevilla, Spain*
[17] *Science Department, Seville University, Av. de la Ciudad Jardín, 20-22, E-41005 Sevilla, Spain*
[18] *Hampshire Astronomical Group, Clanfield, UK*
[19] *Horndean Observatory, 6 Falcon Road, Horndean, Waterlooville, Hampshire PO89BY, UK*
[20] *Royal Astronomical Society, Burlington House, Piccadilly, London W1J 0BQ, UK*
[21] *Bayfordbury Observatory, Department of Physics, Astronomy and Mathematics, University of Hertfordshire, SG13 8LD, UK*
[22] *Wiltshire Astronomical Society, 2 Oathills, Corsham SN13 9NL, UK*
[23] *Bath Astronomers, 19 New King Street, Bath BA1 2BL, UK*
[24] *The Herschel Society, The Herschel Museum of Astronomy, 19 New King Street, Bath BA1 2BL, UK*
[25] *Astronomical Institute, University of Wrocław, ul. M. Kopernika 11, PL-51-622 Wrocław, Poland*
[26] *Astronomical Observatory, University of Warsaw, Al. Ujazdowskie 4, PL-00-478 Warsaw, Poland*
[27] *Volkssternwarte Paderborn, D-33041 Paderborn, Germany*
[28] *Center for Mathematical Plasma Astrophysics, University of Leuven, Oude Markt 13, 3000 Leuven, Belgium*
[29] *Green Island Observatory, Karaoğlanoğlu Street 63A, Geçitkale Mağusa, North Cyprus*
[30] *Observatorio de Sencelles, Sonfred Road 1, E-07140 Sencelles, Mallorca, Spain*

[31]*Selztal Observatory, Bechtolsheimer Weg 26, D-55278 Friesenheim, Germany*
[32]*Centre for Astrophysics Research, University of Hertfordshire, Hatfield AL10 9AB, UK*
[33]*Arkansas Tech University, Russellville, AR 72801, USA*
[34]*Australian National University, Research School of Astronomy and Astrophysics, Mount Stromlo Observatory, Cotter Road, Weston Creek 2611, Australia*
[35]*Department of Data Science and Engineering, Silesian University of Technology, Akademicka 16, PL-44-100 Gliwice, Poland*

This paper has been typeset from a TEX/LATEX file prepared by the author.